Received: 21 April 2017 | Revised: 29 January 2018 | Accepted: 15 February 2018

DOI: 10.1111/bre.12283

ORIGINAL ARTICLE

WILEY Basin Research IAS EAGE

Detrital zircon and apatite constraints on depositional ages, sedimentation rates and provenance: Pliocene Productive Series, South Caspian Basin, Azerbaijan

Nazim R. Abdullayev[1,2] | John Weber[3] | Christiaan G. C. van Baak[4] | Elmira Aliyeva[2] | Caitlin Leslie[5] | Gregory W. Riley[1] | Paul O'Sullivan[6] | Roman Kislitsiyn[7]

[1]BP-Azerbaijan, Xazar Center, Baku, Azerbaijan

[2]Geological Institute of Azerbaijan, Baku, Azerbaijan

[3]Department of Geology, Grand Valley State University, Allendale, MI, USA

[4]Paleomagnetic Laboratory "Fort Hoofddijk", Utrecht University, Utrecht, The Netherlands

[5]Department of Geology, Baylor University, Waco, TX, USA

[6]GSS Services, Moscow, ID, USA

[7]Dahousie University, Halifax, NS, Canada

Correspondence
Nazim R. Abdullayev, BP-Azerbaijan, Xazar Center, Baku, Azerbaijan.
Email: nazim_abdullayev@hotmail.com

Abstract

We used detrital zircon U/Pb geochronology and apatite (U–Th–Sm)/He thermochronology to better constrain depositional ages and sedimentation rates for the Pliocene Productive Series in Azerbaijan. U/Pb analysis of 1,379 detrital zircon grains and (U–Th–Sm)/He analysis of 57 apatite grains—from Kirmaky Valley and Yasamal Valley onshore sections, Absheron Peninsula—yielded two distinct sub-populations: "young" Neogene grains and "old" Mesozoic, Palaeozoic and Proterozoic/Archean grains. The large numbers of Neogene age grains (around 10% of all grain ages) provided a new absolute age constraint on the maximum depositional age of the Lower Productive Series of 4.0 Myr. These "young" Neogene zircon grains most likely originated from volcanic ash falls sourced from the Lesser Caucasus or Talesh Mountains. In this paper we propose a timescale scenario using the maximum depositional age of the Productive Series from detrital zircon grain U/Pb constraints. Potential consequences and limitations of using apatite (U–Th–Sm)/He dating method in estimating maximum depositional ages are also discussed. These new age constraints for the Lower Productive Series gave much faster sedimentation rates than previously estimated: 1.3 km/Myr in the South Caspian Basin margin outcrops and up to 3.9 km/Myr in the basin centre. The sedimentation rates are one of the highest in comparison to other sedimentary basins and coeval to global increase in sedimentation rates 2–4 Myr. The older group of detrital zircon grains constitutes the majority of grains in all sample sets (~80%). These older ages are inferred to reflect the provenance of the Productive Series sediment. This sediment is interpreted to have been derived from the Proterozoic and Archean crystalline basement rocks and Phanerozoic cover of the East European Craton, Proterozoic/Palaeozoic rocks of the Ural Mountains and Mesozoic sedimentary rocks of the Greater Caucasus. This sediment was likely supplied from northerly sourced drainage that emptied into the South Caspian Basin.

1 | INTRODUCTION

Single-grain U/Pb dating of detrital zircon grains is a powerful tool now fairly routinely used to determine the depositional age of clastic sedimentary rocks (Gehrels, Dickinson, Ross, Stewart, & Howell, 1995). It is also useful in provenance studies because it can fingerprint source areas if they have distinctive zircon age populations (Amidon, Burbank, & Gehrels, 2005a,b; Gehrels et al., 1995). Detrital zircons are generally ubiquitous in sandstones because zircon is highly resistant to chemical and physical weathering. Detrital zircons are also useful for dating sedimentary rocks because the U/Pb isotopic system is very robust and is not reset under near-surface conditions. To fully characterize provenance, a full range of ages within detrital grain populations must be determined (Gehrels et al., 2011).

Apatite (U–Th–Sm)/He thermochronology is another effective tool for determining thermal histories of rocks exhumed in orogens (Flowers & Farley, 2012; Reiners & Shuster, 2009). In near-surface sediments and sedimentary rocks, this technique has also been extended to study detrital grains and sediment provenance (Chew & Donelick, 2012; Dunkle, Helmich, & Suslick, 2009).

The closed hydrological nature of the South Caspian Basin leading to faunal endemism during the Pliocene (Aliyeva, Aliyev, Huseynov, Babayev, & Mamedov, 2008), the near absence of any diagnostic fossils that can serve as biostratigraphic markers, and the very thick (>5 km)—broadly Pliocene aged—clastic fill interval (Figure 1), means that alternative absolute age dating methods are needed.

While volcanic ash layers are common in fine-grained deposits in both the Late Miocene (van Baak, Stoica, Grothe, Aliyeva, & Krijgsman, 2016; van Baak et al., 2013) and the Pleistocene, none has been reported in the Pliocene Productive Series. It is thought that the fluvio-deltaic environments of the Pliocene Productive Series did not allow for preservation of in situ ash beds. However, previous studies have highlighted the possibility that significant amounts of erupted volcanic material may have been included in sand consequently deposited into the Caspian Sea Basin (e.g. Forte et al., 2015). This "dilute" volcanic material, if widely distributed, can be used to constrain maximum depositional ages.

As part of a BP-sponsored research programme, 28 outcrop samples from various Pliocene Productive Series sandstones were collected and analysed between 2011 and 2014. These samples come from a wide range of subunits or "suites" that span the entirety of the Pliocene Productive Series, an approximately 1.7 km thick outcrops on the basin margin (Figure 2a). The samples were collected from the cores and flanks of the Kirmaky and Yasamal anticlines, and from the Kirmaky trench, excavated across Kirmaky Valley (Figure 3). This study applies both geochronology and thermochronology techniques and includes U/Pb analysis of 1,387 individual detrital zircon grains and (U–Th–Sm)/He analysis of 57 detrital apatite grains. Detrital zircon grain U/Pb geochronology is used to estimate depositional ages for subunits within the Productive Series. Both detrital zircon U/Pb and apatite (U–Th–Sm)/He geochronology is used to better understand and characterize the provenance of the Productive Series sandstones.

Our new maximum depositional ages are used to better constrain sedimentation rates for onshore outcrops of Productive Series, located on the margins of the South Caspian Basin, and the much thicker offshore deposits in the centre of the South Caspian Basin, using well-established lithostratigraphic correlations.

2 | GEOLOGICAL SETTING

2.1 | Basin evolution

It is thought that the crustal substrate of the South Caspian Basin formed as a Mesozoic back-arc extensional basin behind the Lesser Caucasus–Talesh arc, in response to north-directed subduction and associated slab rollback of Neo-Tethys seafloor (Allen, Vincent, Alsop, Ismail-Zade, & Flecker, 2003; Khain, 1975; Zonenshain & Le Pichon, 1986). Since its formation, the South Caspian Basin has gradually evolved in to an isolated and enclosed (lake) basin that has experienced extreme shifts in lake level. During the Oligocene and Miocene, its semi-closed nature and periodic anoxic conditions led to deposition of the prolific Maykop and Diatom Suite petroleum source rocks in the Paratethys lake (Figure 1). The basin then experienced an increase in sedimentation rate thought to be associated with post-Oligocene orogeny in the Caucasus, as a result of the (still ongoing) collision between the Eurasian and Arabian plates (Abdullayev, Kadirov, & Guliyev, 2015; Allen et al., 2003; Avdeev & Niemi, 2011; McClusky et al., 2000; Reilinger et al., 2006; Vernant et al., 2004). The final isolation of the South Caspian Basin culminated with the deposition of the Pliocene Productive Series, also associated with a significant increase in sedimentation rate (Abdullayev, Riley, & Bowman, 2012; Aliyeva et al., 2008; Azizbekov, 1972; Baturin, 1937; Salmanov, Suleymanov, & Maharramov, 2015). This final isolation event appears to be to synchronous to rapid Pliocene exhumation in the Caucasus (Avdeev & Niemi, 2011; Nummedal, Clifton, & Williams, 2012). The increase in sedimentation rate is thought to be the result of a fall in Caspian base level

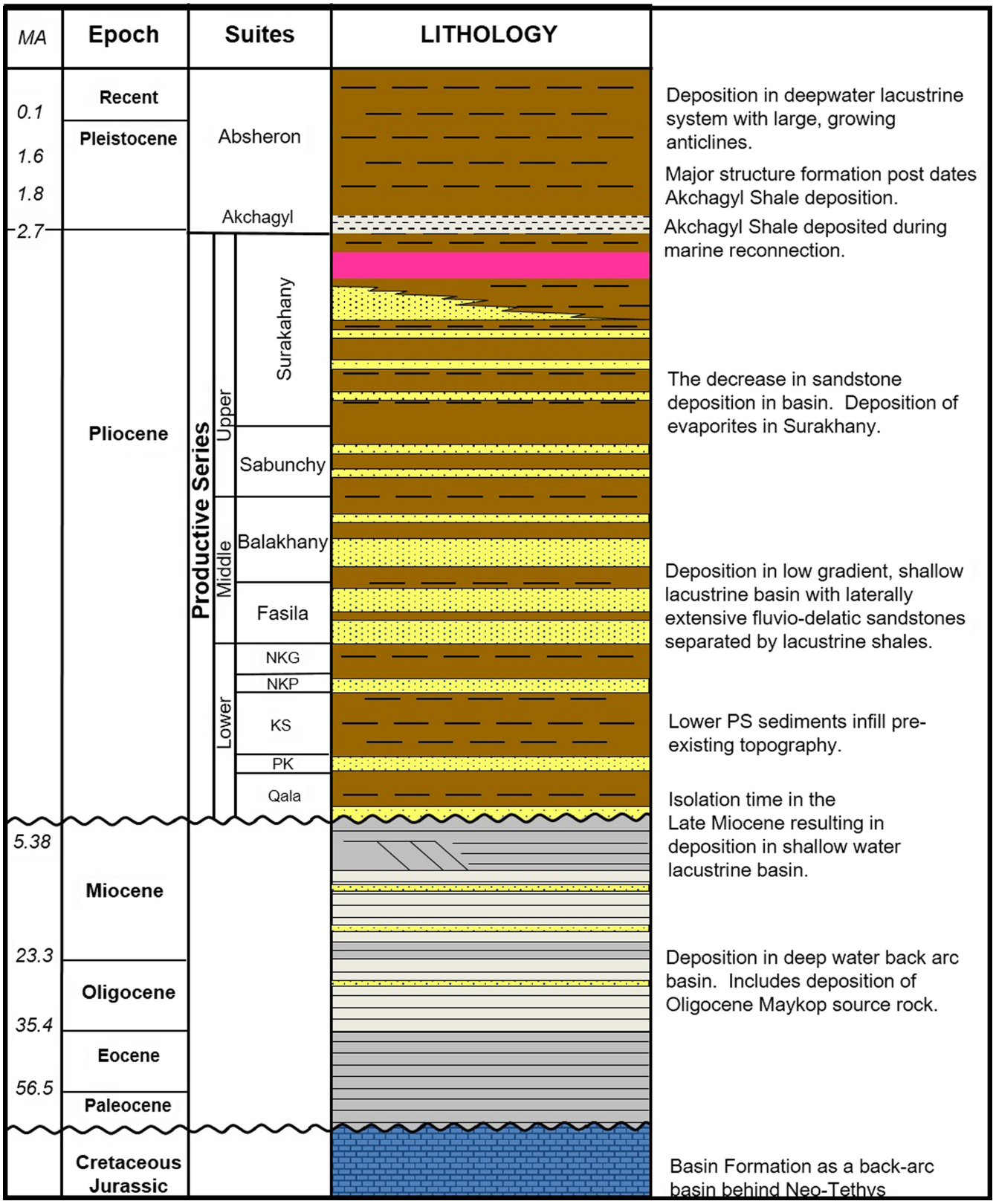

FIGURE 1 Stratigraphic column for the South Caspian Basin, highlighting evolution from the basin inception to present day. Productive Series naming convention of the lithostratigraphic suites includes some Russian language abbreviations: PK (Under Kirmaki Sandy), KS (Kirmaki) NKP (Above-Kirmaki Sandy), NKG Sute(Above Kirmaki Shaly)

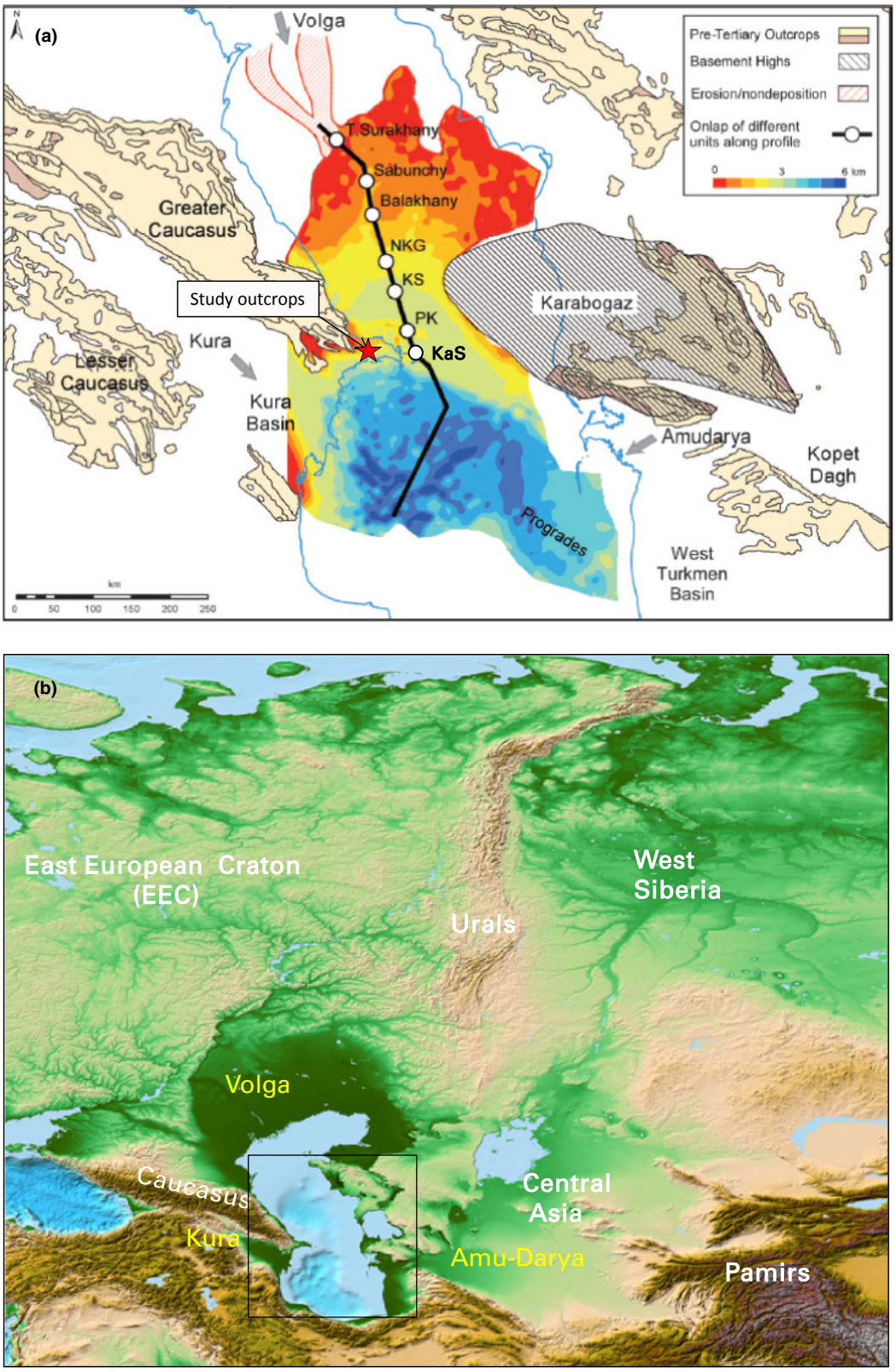

FIGURE 2 (a) Uncompacted isopach thicknesses of Productive Series (map modified from Abdullayev et al., 2012) range from 1.7 to 2 km on the basin margin in the study area to 6 km offshore South Caspian. White circles indicate progressive onlaps of depositional units on the master erosional surface at the base of PS. These stratigraphic onlaps are labelled as KaS = Qala Suite (only observed from wells and seismic), PK = Post-Kirmaky Sandy suite, KS = Kirmaky Suite, NKG = Post Kirmaky Shaly Suite; (b) – Topographical map of Central Eurasia, with the sediment provenance areas for Pliocene Productive Series and river systems delivering sediments in Pliocene. Black rectangle indicates location of Figure 2a

(maximum of 1–1.5 km) and establishment of the connection to sediment-rich drainage systems. This involved the incision of the Palaeo-Volga river and Palaeo-Amudarya river canyons (Figure 2), and the integration of drainage systems from the East European Craton, Urals and Central Asia and Caucasus (Abdullayev et al., 2012; Reynolds et al., 1998;).

This increased sediment delivery-rate, resulted in the deposition of >5 km of lacustrine and fluvio-deltaic fill that comprise the Pliocene Productive Series (Abdullayev et al., 2012; Figure 2a). The Pliocene Productive Series is therefore interpreted to be a low stand systems tract, that formed as a consequence of a major base-level fall (Nummedal et al., 2012). The depositional fill of the Productive Series produced stratal geometries apparently controlled by relative changes in lake level and local changes in sediment supply. The Productive Series bounding surfaces record the closure of connections between the Caspian and Black Seas (top of Upper Miocene Pontian Formation) and the subsequent reconnection of the South Caspian Basin to the world's oceans (top of the Surakhany Suite, uppermost Productive Series, and in the overlying Akchagyl Suite; Abdullayev et al., 2012).

Because of this rapid and largely terrestrial infill event, fossils and biostratigraphic controls are rare or lacking in the Productive Series (Popov et al., 2006). Nonetheless, these rocks have been subdivided into units that are called "suites" in the old Soviet terminology (Azizbekov, 1972; Baturin, 1937; Potapov, 1954; Sultanov, 1949) using a lithostratigraphic approach (Figure 1). These subdivisions can be reliably correlated between onshore outcrops, and from onshore to offshore oil and gas fields. In detail, the Lower Productive Series (excluding the lowermost Qala Suite that is only known from wells) outcrops at Kirmaky Valley and include (i) the pre- (below-) Kirmaky Sandy Suite (PK), (ii) the Kirmaky Suite (KS), (iii) above-Kirmaky Sandy Suite (NKP) and (iv) above-Kirmaky mudstone Suite (NKG). The Middle and Upper Productive Series include (v) the Fasila Suite outcropping in Kirmaky Valley and (vi) the Balakhany, (vii) Sabunchy and (viii) Surakhany suites that outcrop in Yasamal Valley (Figure 2). Average thicknesses of these suites around the Absheron Peninsula are as follows: PK is around 40–60 m thick, KS is 150–250 m thick, NKP is around 50 m thick, NKG is 50 m thick, Fasila to Balakhany suites total to around 500 m, Sabunchy Suite is 250 m thick and Surakhany Suite is between 500 and 1,000 m thick (Azizbekov, 1972; Salmanov et al., 2015).

2.2 | Constraints on the age of the Productive Series

The precise relationship between the Pliocene Productive Series suites and global timescales has been, and still is, the subject of much debate. A number of direct and indirect methods have been employed to clarify this relationship. van Baak et al. (2013) provided a comprehensive review of the previously proposed Productive Series timescales with their respective shortcomings.

Until now, absolute age controls have been sparse and previous attempts to correlate the Productive Series to global records have employed the weak biostratigraphic controls available. Age estimates have also been made using recognized discrete patterns and cycles from climatic arguments and sequence stratigraphy (Abdullayev et al., 2012; Abreu & Nummedal, 2007; Green, Abdullayev, Hossack, Riley, & Roberts, 2009; Nummedal et al., 2012). The lack of absolute age constraint for the Productive Series makes these correlations somewhat ambiguous. Age constraints for the lower and upper boundaries of the Productive Series should also rely on the available geochronological studies of the over- and underlying sediments.

Productive Series strata are underlain by highstand deposits of the Pontian regional stage (Abdullayev et al., 2012; van Baak et al., 2016). The Pontian stage can be traced throughout the Paratethys realm with important deposits present in the Dacian Basin of Romania (Stoica et al., 2013), the Black Sea (Chang et al., 2014; Krijgsman, Stoica, Vasiliev, & Popov, 2010) and the circum-Caspian Sea (van Baak et al., 2016). The base of the Pontian stage is characterized by a marine flooding event dated at 6.1 Ma by means of integrated bio-magnetostratigraphic and cyclostratigraphic dating (van Baak et al., 2016). Using the most recent Global Polarity Time Scale (Hilgen, Lourens, & van Dam, 2012), the majority of the Pontian stage correlates to the long C3r chron, between 6.033 Ma and 5.235 Ma (van Baak et al., 2016; Krijgsman et al., 2010; Vasiliev et al., 2004). Cyclostratigraphic tuning of the Ajiveli section in the Gobustan region of Azerbaijan, dates the top of the Pontian stage to younger than 5.38 Ma (van Baak et al., 2016). This age is therefore seen as an important maximum constraint for the age of the base of the Productive Series.

Prior to the current study, a variety of different radiometric dates for ash beds near the lower boundary of the Akchagyl, which marks the top of Productive Series, have been reported or assumed. These vary from 3.4 to 3.2 Ma (Devlin et al., 1999; Vincent, Davies, Richards, & Aliyeva, 2010) and 2.4 to 2.6 Ma (Abdullayev, 2000). Abdullayev et al. (2012) and Green et al. (2009) both used the 2.6 Ma date to mark the top of the Productive Series. Since then, van Baak (2015) used high-resolution magnetostratigraphy, integrated with $^{40}Ar/^{39}Ar$ dating of a series of volcanic ash beds in sediment overlying Akchagyl flood beds at outcrops located near Jeirankechmez River (Figure 3a). This gave an age for the upper

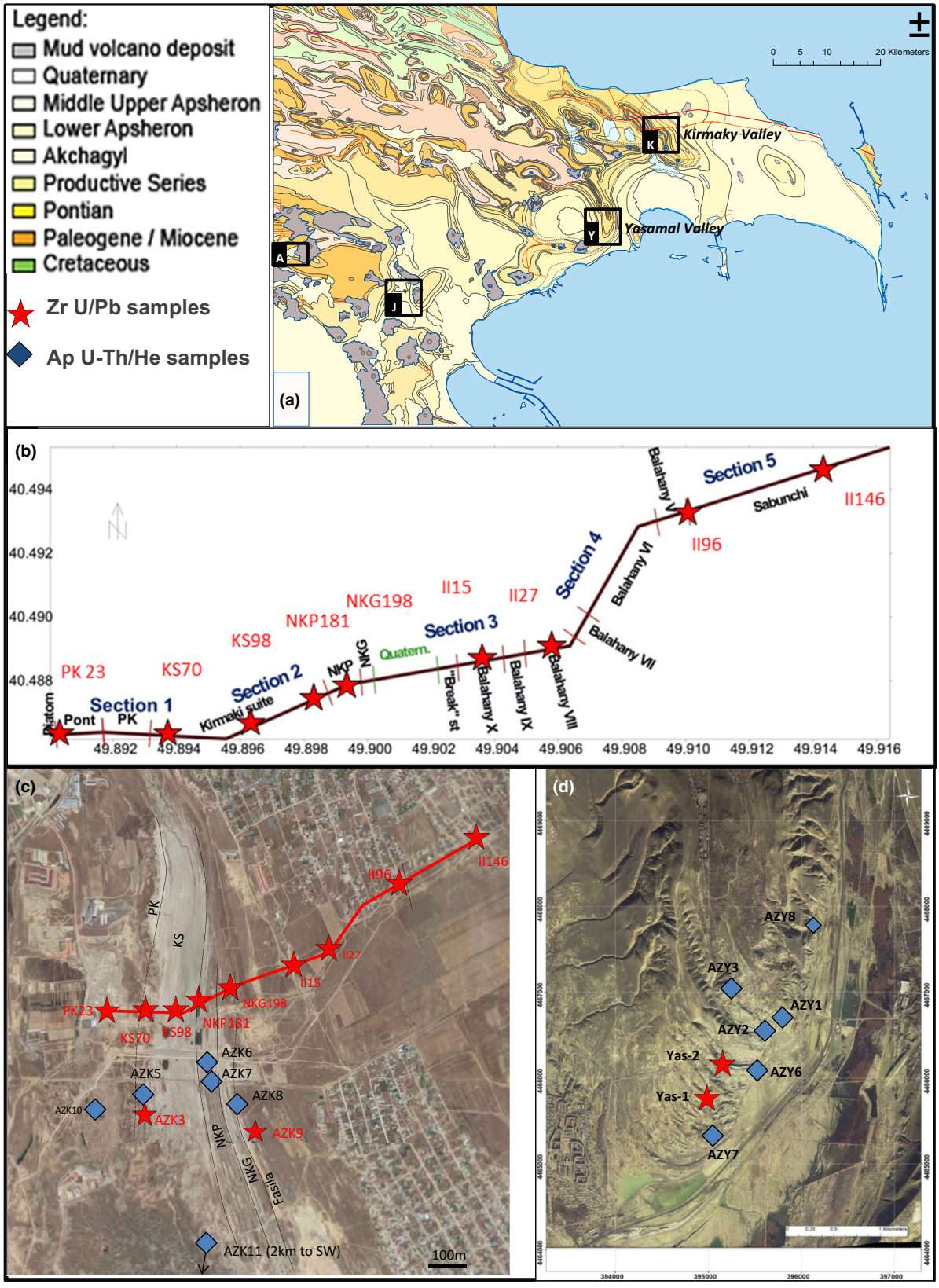

FIGURE 3 Geographic locations of outcrops and sampling programme. (a) - Geological Map of Azerbaijan modified from van Baak (2015) that includes outcrops with available age constraint on Pliocene Productive Series. These outcrops are Ajiveli (A), Jeyrankechmez (J) Kirmaky (K), Yasamal (Y), (b) - Position of the trench section dug through the Kirmaky Valley with sampling locations and stratigraphic boundaries, (c) - Satellite map of Kirmaky Valley showing trench transect from b), zircon U/Pb samples (red stars) and apatite U-Th/He samples (blue diamonds). (d) – Satellite map of the Yasamal Valley with locations of zircon U/Pb samples (red starts) and apatite U-Th/He samples (blue diamonds)

boundary of the Productive Series of 2.71 ± 0.02 Ma, which we adopted in this study.

2.3 | Sandstone provenance

During the deposition of the Pliocene Productive Series, the main sediment sources supplying clastics to our study area in the Absheron Peninsula, Azerbaijan were the East European Craton (Russian Platform), the Urals and the Greater and Lesser Caucasus (Abdullayev et al., 2012; Aliyev, 1949; Reynolds et al., 1998; Figure 2b). The heavy mineral assemblages of some of these source regions were previously determined by analysing modern river sediments and outcrops in the Absheron Peninsula. Kirmaky and Yasamal valley outcrops were also sampled, somewhat sparsely, for heavy minerals and detrital zircon U/Pb to determine provenance (Allen, Morton, Fanning, Ismail-Zadeh, & Kronenberg, 2006; Morton et al., 2003).

The Russian Platform or East European Craton (EEC) sediment source is characterized by Archean and Proterozoic rocks as well as Palaeozoic and Mesozoic input (Allen et al., 2006; Figure 2b). Archean and Proterozoic age rocks are mostly metamorphic (biotite–garnet-gneiss, amphibolite and schist); these are heavily recycled throughout EEC (Allen et al., 2006). Palaeozoic and Mesozoic age rocks are characterized by quartz-rich sandstones containing the recycled Archean or Proterozoic grains and some carbonate (Abdullayev & Leroy, 2016; Allen et al., 2006). Lesser Caucasus sourced sediments are mostly derived from Jurassic, Cretaceous, Palaeogene and Neogene age arc-volcanic rocks: lava flows, diabase and volcanoclastic rocks with limestones including terrigenous carbonaceous-flysch (Abdullayev & Leroy, 2016). The Greater Caucasus source is characterized by Jurassic and Cretaceous-aged quartz-sandstones and mudstones, with minor reef limestones and terrigenous carbonaceous flysch (Abdullayev & Leroy, 2016; Buryakovsky, Chilingar, & Aminzadeh, 2001; Mosar et al., 2010).

Most of the Productive Series sandstones exposed in the Absheron Peninsula (Kirmaky, Yasamal and Lokbatan Valleys) were derived from the north by the Palaeo-Volga Ural system and are quartz-rich (Abdullayev et al., 2012; Allen et al., 2006). Morton et al. (2003) also reported a significant increase in Eastern Greater Caucasus mineral assemblages in later Productive Series deposition that they interpret as related to increased exhumation and erosion of this mountain range during the Pliocene. An alternative explanation for the increase in the Greater Caucasus contribution to the Productive Series sediment is a climate change in the sediment source area during Productive Series deposition (Abdullayev & Leroy, 2016). Abdullayev and Leroy's (2016) analysis of clay mineral assemblages agree with Morton et al. (2003) and Allen et al. (2006), concluding that the Lower Productive Series was sourced from mostly Palaeo-Volga sediment, and the Upper Productive Series was sourced from mixed Palaeo-Volga and Greater Caucasus provenances.

Heavy mineral assemblages from Productive Series outcrops in the south-eastern area of Azerbaijan show similar characteristics to sands from the modern Kura River (Morton et al., 2003). They are consistent with having been derived from sediments from Mesozoic age volcanic rocks of the Lesser Caucasus. Morton et al. (2003) also noted a change in sediment characteristics from some of the Surakhany Suite outcrops southwest of Yasamal (Aktapa Bridge location). The change in mineralogy associated with the Surakhany Suite implies that there was a redistribution of fluvial drainage patterns at that time, with the influence of the palaeo-Kura increasing at the expense of the palaeo-Volga. The bulk of the Surakhany strata in the Absheron Peninsula are fine grained, indicating that the palaeo-Volga was more distal at this time, or had shifted to a finer-grained bedload (Hinds, Simmons, Allen, & Aliyeva, 2007).

2.4 | Greater Caucasus surface uplift and exhumation

Apatite fission-track analysis (AFT) of the Greater Caucasus Maykop Series has previously shown an Oligocene–Miocene age (Alpine) start of orogenesis in the Greater Caucasus, with the earliest uplift occurring in the core of the range (Philip, CisternaS, Givshiani, & Gorshkov, 1989; Vincent, Morton, Carter, Gibbs, & Barabadze, 2007; Vincent et al., 2011). Additional studies conducted in the central and eastern parts of the Greater Caucasus (e.g. Niemi & Avdeev, 2010; Avdeev & Niemi, 2011; Kral & Gurbanov, 1996) also demonstrated increased AFT cooling rates during the Oligocene. Cooling rates then remained relatively constant until the Lower Pliocene, when they rapidly increased to 25°C/Myr in the central Caucasus and up to 10°C/Myr in the eastern Caucasus. The recorded cooling onset occured ca. 20 Ma, with a rapid increase of 5 Ma that is coeval with the deposition of the Productive Series. Avdeev (2011) analysed a N–S cross-section (48°E) in the Azerbaijani portion of the northern Caucasus and determined the maximum magnitude of exhumation in this part of the range to be around 4 km**.** Avdeev (2011) further interpreted that such exhumation was caused by significant tectonic shortening during collision between the Eurasian Plate and the Lesser Caucasus. They suggested a maximum denudation rate of 800–1,000 m/Myr. Another AFT

analysis (Mosar et al., 2010), suggested an age of uplift of 21.8 Ma from samples taken from Jurassic sandstone north of Shahdag Mountain, Azerbajan. Both results imply that strong Cenozoic surface uplift likely occurred in the Eastern Caucasus.

3 | OUTCROP LOCATIONS AND SAMPLES

3.1 | Kirmaky Valley

The Kirmaky outcrops we sampled are about 12 km northeast of Baku in a wind-deflated valley with excellent and continuous exposures (Figure 3a). Kirmaky Valley is developed on the east flank of the Kirmaky anticline. The core of the anticline contains poorly exposed Pontian marls. The eastern-fold limb, largely unbroken by faults, forms a homocline dipping moderately to steeply to the east. Individual resistant sandstone beds protrude as wind-sculpted ribs in the valley (i.e. yardangs). Many individual beds can be traced for tens to hundreds of metres along strike. The north–south orientation of Kirmaky Valley is broadly parallel to the mean palaeocurrent direction providing a depositional dip-oriented view of these units (Hinds et al., 2007). Units exposed range from PK sandstone on the west side of the valley to the Fasila and Balakhany Suite intervals on the east side of the valley (Figure 3). No outcrops of the Qala Suite, which forms a major reservoir unit nearshore and offshore, have been found or reported here, or elsewhere on the Absheron Peninsula.

In 2006, a pipeline trench (generally referred to as the Kirmaky trench) was excavated across the Kirmaky Valley creating fresh exposures that were nearly continuously sampled and gamma ray logged from the Kirmaky Suite to the Sabunchy Suite (Figure 3b,c). The Kirmaky trench represents the most continuous and complete outcrop of the Productive Series found to date in onshore Azerbaijan and compliments the abundant onshore and offshore well logs available through this interval. The gamma-ray log from the trench records almost 1,300 m of continuous section, being only incomplete between NKP and Balakhany Suites, due to poor exposure (Figure 4). The new gamma-ray log from the trench is nearly identical to the gamma-ray log previously taken directly from the natural outcrops in the valley (Abreu & Nummedal, 2007). Additionally, the Kirmaky trench gamma-ray log records variations in sand/shale ratios that are almost identical to those seen in many of the offshore wells and helps to demonstrate that the suites in the Lower Productive Series are laterally extensive and continuous, and can be correlated across long distances (Abdullayev et al., 2012; Reynolds et al., 1998). Sedimentary log shows lithologic characteristics that are generally similar to other sections of the Pliocene Productive Series in the Absheron peninsula, e.g. those based on measured sections at Kirmaky valley and Yasamal Valley and Lokbatan outcrops, as compiled by Hinds et al. (2007) from several sources, including Aliyev (1949), Azizbekov (1972) and Jones and Simmons (1996).

Eight samples were collected from natural outcrops and analysed in 2011. Two natural outcrop samples were collected for detrital zircon U/Pb dating (2011–AZ–K3 & 2011–AZ–K9; orange stars in Figure 4). Sample 2011–AZ–K3 was collected from the base of the Kirmaky Suite from the top of the PK unit. Sample 2011–AZ–K9 was collected from the base of the Fasila Sandstone unit, a distinctive conglomeratic sandstone in the Productive Series (Figure 3). Nine additional Kirmaky Valley samples (PK23, KS70, KS98, NKG198, NKP181, II–15, II–27, II–99 and II–146) were collected from the Kirmaky trench and analysed for detrital zircon U/Pb dating in 2014 (red stars in Figures 3b and 4). The stratigraphically oldest sample was collected from the PK sand (sample PK23) and the youngest sample, II–146, was collected from what could be the Sabunchy or earliest Surakhany Suite. Grains from six samples: 2011–AZ–K5 (lower Kirmaky Suite); 2011–AZ–K6 (top Kirmaky Suite); 2011–AZ–K7 (base NKG); 011–AZ–K8 (mid-NKG); 2011–AZ–K10 (Kirmaky Suite) and 2011–AZ–K11 (Balakhany) were also collected in 2011 and analysed *via* apatite (U–Th–Sm)/He thermochronology (Figure 4).

3.2 | Yasamal Valley

Upper Productive Series strata are exposed near Yasamal Valley, about 10 km west of Baku (Figure 3d). The strata are best exposed in a section along the southern nose of the south-southeast plunging Yasamal Anticline. The east–west orientation of this exposure gives an essentially depositional strike-parallel exposure. According to well-established geological correlations, the Balakhany and Sabunchy Suites correlate to the subunits exposed at Yasamal Valley (Hinds et al., 2007). However, precise stratigraphic correlations between the Yasamal Valley outcrops and the Kirmaky trench are not well established; no good marker beds exist for the Yasamal Valley exposures. Recently a gamma-ray log was acquired in the upper part of the exposure of Yasamal valley in what could be either the Sabunchy or the Surakhany suite (Figure 4).

Two samples were collected for detrital zircon U/Pb analysis from Yasamal Valley (Yas–1 and Yas–2; Figure 3d) and analysed in 2014. Apatite grains from six

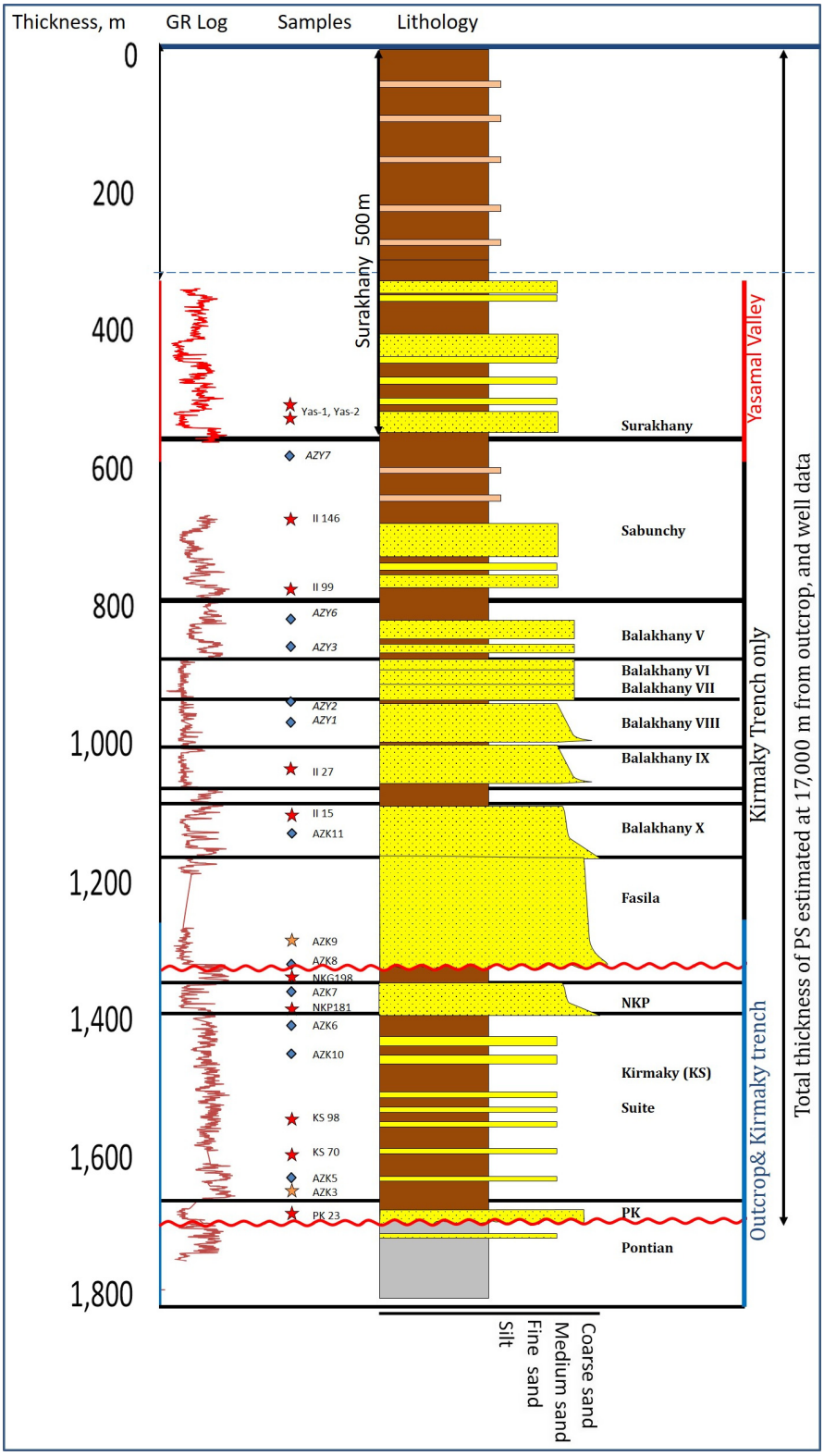

FIGURE 4 Composite stratigraphy of Productive Series based on Aliyev (1949), Hinds et al., (2007) with gamma-ray log and sedimentary log, based on the measured sections from Kirmaky trench, Kirmaky Valley outcrops and Yasamal Valley outcrops. Figure illustrates stratigraphic position of the Zr U/Pb samples (orange stars for Kirmaky outcrops samples collected in 2011 and red stars for Kirmaky trench samples collected in 2014) and apatite U-Th/He samples (blue diamonds)

samples were analysed using apatite (U–Th–Sm)/He: 2011–AZ–Y–1 (Balakhany); 2011–AZ–Y–2 (Balakhany); 2011–AZ–Y–3 (Balakhany); 2011–AZ–Y–6 (Balakhany); 2011–AZ–Y–7a (possibly Surakhany) and 2011–AZ–Y–7b (Surakhany; Figure 3c). All of apatite grain samples were analysed in 2011.

4 | METHODS

4.1 | General sample preparation

All sample processing and analytical work, was undertaken by Apatite to Zircon, and GeoSep Services (GSS), Idaho,

USA. Mineral grains were isolated and prepared for LA-ICP-MS analysis using standard procedures combined with specific customized procedures described by Donelick, O'Sullivan, and Ketcham (2005).

4.2 | U/Pb LA-ICP-MS method

Descriptions of the methods followed to produce and process zircon U/Pb data have been presented in Bradley et al. (2009), Hultz, Wilson, Donelick, and O'Sullivan (2013) and Moore, O'Sullivan, Potter, and Donelick (2015). Zircons (both standards and unknowns) were mounted in epoxy wafers and ground and polished to expose internal grain surfaces. Grains, and the locations for laser spots were selected for analysis using transmitted light with an optical microscope at 2,000× magnification, which allows the recognition and characterization of features below the surface of individual grains.

Isotopic analyses were performed with a New Wave UP-213 laser ablation system in conjunction with a Thermo-Finnigan Element2 single collector double-focusing magnetic sector inductively coupled plasma mass spectrometer (LA-ICP-MS) in the GeoAnalytical Lab at Washington State University. For all laser analyses, the beam diameter was 20 μm and the frequency was set at 5 Hz, yielding ablation pits ~12–15 μm deep. He and Ar gas were used to deliver the ablated material into the plasma source. Each analysis of 200 cycles took approximately 30 s to complete and consisted of a 6-s integration on peaks with the laser shutter closed (for background measurements) followed by a 25-s integration with the shutter open. A 30-s delay occurred between analyses. The isotopes measured included 202Hg, 204(Hg + Pb), 206Pb, 207Pb, 208Pb, 232Th, 235U and 238U. The Element2 detector was set at analogue mode for 232Th and 238U and at pulse counting mode for all other isotopes.

Previous LA-ICP-MS studies of UPb zircon dating used the "intercept" method, which assumes that isotopic ratio varies linearly with scan number due solely to linearly varying isotopic fractionation (Chang, Vervoost, McClelland, & Knaack, 2006; Gehrels, Valencia, & Ruiz, 2008). The data modelling approach favoured here was the modelling of background-corrected signal intensities for each isotope at each scan. Background intensity for each isotope was calculated using a fitted line (for decreasing background intensity) or using the arithmetic mean (for non-decreasing background intensity) at the global minimum of selected isotopes (206Pb, 232Th and 238U) for the spot. Background+signal intensity for each isotope at each scan was calculated using the median of fitted (second-order polynomial) intensity values for a moving window (7 scans wide here) that includes the scan. The precision of each background-corrected signal intensity value was calculated from the precision of background intensity value and the precision of the background+signal intensity value.

A number of zircon U/Pb age standards were used during analysis for calibration purposes. These included the 1099 ± 0.6 Ma FC zircon (FC-1 of Paces & Miller, 1993) as the primary age standard. The secondary age standard was the 61.2 ± 0.1 Ma Tardree Rhyolite zircon (Dave Chew, *personal communication*). Third-level age standards included the Fish Canyon Tuff with an age of 28.20 ± 0.1 Ma (Lanphere & Baadsraard, 2001), the Mount Dromedary Syenite with an age of 99.1 ± 0.1 Ma (Renne et al., 1998) and the Temora2 diorite with an age of 416.8 ± 0.3 Ma (Black et al., 2004). At the beginning of the LA-ICP-MS session, zircon standards (TR and FC1) were analysed until fractionation was stable and the variance in the measured 206Pb/238U and 207Pb/206Pb ratios was at or near 1%. In order to correct for inter-element fractionation during the session, these standards were generally reanalysed after each 15–25 unknowns. Uranium decay constants and the 238U/235U isotopic ratio reported in Steiger and Jäger (1977) were used.

Uranium decay constants and the $^{238}U/^{235}U$ isotopic ratio reported in Steiger and Jäger (1977) were used in this study. $^{207}Pb/^{235}U_c$ ($^{235}U_c = 137.88^{238}U$), $^{206}Pb/^{238}U$ and $^{207}Pb/^{206}Pb$ ages were calculated for each data scan and checked for concordance; concordance here was defined as overlap of all three ages at the 1σ level (the use of 2σ level was found to skew the results to include scans with significant common Pb). The background-corrected isotopic sums of each isotope were calculated for all concordant scans. The precision of each isotopic ratio was calculated by using the background and signal errors for both isotopes. The fractionation factor for each data scan, corrected for the effect of accumulated α-damage, was weighted according to the ^{238}U or ^{232}Th signal value for that data scan; an overall weighted mean fractionation factor for all concordant data scans was used for final age calculation.

If the number of concordant data scans for a spot was greater than zero, then either the $^{206}Pb/^{238}U$ (for ages <1.5 Ga) or $^{207}Pb/^{206}Pb$ (for ages >1.5 Ga) age was chosen as the preferred age. If zero concordant data scans were observed, then the analysis was deleted. Common Pb was subtracted out using the Stacey and Kramer (1975) common Pb model for Earth. Ages and common Pb ratio were determined iteratively using a preset, session-wide minimum common Pb age value (default for each session was the age of the oldest age standard which for both apatite and zircon was 1099 Ma FC-1 and/or FC-5z).

4.3 | (U–Th–Sm)/He method

Apatite grains were concentrated at the Apatite To Zircon Laboratory using the heavy liquid and magnetic separation

techniques described in section 4.1. Grain selection is a very important step for the (U–Th–Sm)/He analysis. All of the apatite grains selected for this study were handpicked by Ray Donelick at the Apatite To Zircon Laboratory using a high-magnification stereoscopic microscope. Primary selection was done under plane-polarized light and final selection and quality control was done under cross-polarized light. Preference was given to the most euhedral, transparent, crack- and inclusion-free grains with the smallest dimension being not less than 70 mm. Grains selected for analysis were photographed and measured before sealing them into 1 × 1 mm platinum tubes. These measurements were used to calculate grain surface area, grain volume and α-ejection correction based on surface to volume ratio (Farley, Wolf, & Silver, 1996).

(U–Th–Sm)/He analysis includes two major steps being (i) non-destructive extraction and measurements of daughter ^{4}He and (ii) dissolution of the minerals and measurements of parent ^{238}U, ^{235}U, ^{232}Th, and ^{147}Sm isotopes. Roman Kislitsyn completed all this work at the (U–Th–Sm)/He Thermochronometry Laboratory, University of Texas, Austin, USA. Details of the (U–Th–Sm)/He methods used are given in Blackburn, Stockli, Carlson, and Berendsen (2008) and Bidgoli et al. (2015), as well as on the University of Texas Thermochronology Laboratory website (http://www.jsg.utexas.edu/he-lab/u-thhe-noble-gas-lab/) and are next outlined below.

Helium extraction and measurement was completed using a home-built He extraction line, equipped with 75 W diode laser and quadrupole mass spectrometer. Each platinum packet, containing a single grain of apatite, was heated to 1,050°C for 5 min to release ^{4}He trapped in the crystal. The sample He was then spiked with a precisely measured aliquot of ^{3}He and the ^{3}He/^{4}He ratio was then measured using a quadrupole mass spectrometer. This procedure was repeated to make sure no He was left in the grain. Only grains that displayed a blank amount of ^{4}He after the re-extraction were taken for further analyses. Typical errors for the apatite He analyses are in the range of 0.1%–0.5% (1σ), sometimes reaching 1.5%, and in rare cases even higher. Samples were analysed in groups of 44, the maximum number of spots on the laser planchette. Each group of samples included two or three Durango standard apatites. These standards were processed in exactly the same way as unknown samples to ensure accuracy and reproducibility of the data.

For parent isotopes analysis, apatite grains were spiked with a mixed ^{235}U-^{230}Th-^{149}Sm spike and dissolved in 7 N nitric acid at 80°C for 90 min. The 7 N sample solution was diluted to 5% in preparation for the ICP–MS analysis. At this stage, two spiked blanks and two spiked normal solutions were added to ensure analytical precision. Normal solution contained 1 ppm of each U, Th, and Sm of natural isotopic composition. Spiked normal solutions were used to calibrate spike concentration and to ensure it did not change over time due to evaporation.

U, Th and Sm isotope ratios were analysed using a Fisher Scientific Element2 machine at the (U–Th–Sm)/He Thermochronometry Laboratory. Isotopes ^{147}Sm, ^{149}Sm, ^{230}Th, ^{232}Th, ^{235}U and ^{238}U were measured in low-resolution mode with intensities ranging from first tenths-of-thousands cps to first millions of cps, depending on the sample. Measured peak intensities were corrected for mass fractionation and blanks by Element2 software. Typical isotope ratios errors range from 0.1% for high intensity peaks, up to 1% and more for low intensity peaks.

All raw data were reduced using a Helios software package developed by R. Kislitsyn and D. Stockli specifically for (U–Th–Sm)/He data reduction. An α-ejection correction was calculated based on the surface to volume ratio (Farley et al., 1996). Cooling ages were calculated using the He ingrowth equation from Farley (2002).

4.4 | Method for determining maximum depositional ages

In a study designed to test a suite of different strategies for determining maximum depositional ages using detrital zircon U/Pb data, as well as to assess the subsequent resulting accuracies, Dickinson and Gehrels (2009) outlined four alternate methods, using: (a) simply the youngest single grain age; (b) the youngest graphical age peak controlled by more than one-grain age; (c) the mean age of the youngest two or more grains that overlap in age at 1σ and (d) the mean age of the youngest three or more grains that overlap in age at 2σ. These methods range from least (a) to most (d) statistically robust. Despite indicating that method (a) is the least statistically robust, Dickinson and Gehrels (2009) stated that this method was compatible with depositional ages for a majority of samples studied. Method (d) is a more conservative way to represent a "pooled" youngest detrital zircon age.

For all of our detrital zircon ages and apatite ages evaluated (Table 1) we follow Dickinson and Gehrels (2009) and determine and evaluate multiple possible maximum depositional ages using two of their methods: (i) first, based on the single youngest grain in the population that is potentially an underestimate of the maximum depositional age (method (a) above) and (ii) second, using a more conservative approach by calculating the weighted mean age of the youngest population overlapping in age within 2σ (method (d) above). The University of Arizona Laserchron Center, USA, AGEPICK program was used for this second approach as described by Dickinson and Gehrels (2009). Resulting weighted-mean ages are not too different from the arithmetic averages of the youngest population,

overlapping at age within 2σ that we also calculated and used for comparison. Using method (d), the analysed single-grain ages are checked for consistency by comparing the relationships between age and the measured uranium concentration (U_{conc} in ppm) and U/Th ratio.

5 | RESULTS AND INTERPRETATION

5.1 | Detrital U/Pb zircon ages

5.1.1 | U/Pb summary

U/Pb detrital zircon grain analysis of 13 Pliocene Productive Series samples, collected between 2011 and 2014, yielded 1,379 separate grain ages (Table 1). Firstly, our detrital zircon single-grain ages were grouped into Neogene, Mesozoic or Palaeozoic, Proterozoic and Archean age bins (Figure 5). The average analysed grain count for a single detrital zircon sample was just over 100 grains per sample, ranging between 95 and 116 (Table 1), resulting in good age statistics. The oldest age for an analysed detrital zircon grain was 2.9 Gyr; the youngest age obtained was 3.86 Myr. Forty per cent of grains are Proterozoic age, 39% are Palaeozoic age, 13% are Mesozoic age and around 8% are Neogene age. The analytical error (2σ) for the single grain detrital zircon U/Pb ages typically range from less than ±0.48 Myr for the Neogene age grains to around ±40 Myr for the Archean age grains. For Neogene ages, this translates into an average error of ~11%, and for the older grains, the average error reduces to ~1.6%.

To summarize, two distinct populations of detrital zircon grains were identified: "old" grains from Mesozoic to Archean in age, from which provenance information could be derived and "young" Neogene age grains, which could constrain age of Pliocene Productive Series. The absence of Palaeogene age grains creates a distinct gap in the age record (Figure 5)—no single-grain ages were obtained from any of our samples that ranged in age between 10 Ma and the Cretaceous.

5.1.2 | "Old" grain group and provenance patterns

Our interpretation of the U/Pb detrital zircon grain provenance of the Pliocene Productive Series sandstones builds on the work of Allen et al. (2006), with the major difference being the sample size used in this study, at around 100 ages per sample, which is about double of that used by Allen et al. (2006). We also used a larger number of samples that are more evenly spaced through the Productive Series (Figure 2). These differences allow us to interpret and discuss provenance patterns in more detail than has been previously possible.

TABLE 1 Zr U/Pb grain ages count from Kirmay and Yasamal outcrop samples

Sample name	PK23	AZK3	70-KS	13-KS	181-NKP	198-NKG	AZK9	II-15	II-27	II-99	II-146	Yas-1	Yas-2	Total number of individual grain ages	Percentage of total
Formation	PK	Kirmaky	KS	KS	NKP	NKG	Fasila	Bal IX	Bal VIII	Sabunchy	Sabunchy	Sabunchy	Surakhany		
Neogene	14	7	8	13	9	3	15	9	15	6	5	0	4	108	7.8
Palaeogene	0	0	0	0	0	0	0	0	0	0	0	0	0	0	0.0
Mesozoic	11	4	17	19	24	12	9	18	16	15	11	10	12	178	12.9
Palaeozoic	32	27	49	62	51	36	19	67	55	32	61	17	36	544	39.4
Proterozoic	48	64	30	9	20	38	61	11	24	38	26	63	54	486	35.2
Archean	5	7	5	4	5	2	10	2	6	4	4	5	4	63	4.6
Total	110	109	109	107	109	91	114	107	116	95	107	95	110	1,379	

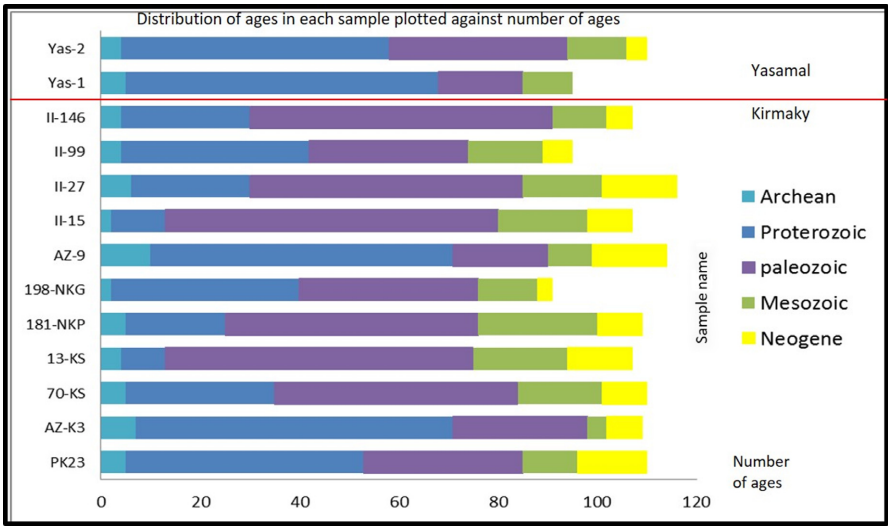

FIGURE 5 Detrital zircon (U/Pb) summary graph showing distribution of the grain ages on from the oldest sampled stratigraphic unit (PK–23) at Kirmaky Trench to the youngest in Yasamal Valley (Yas-1)

To interpret sediment provenance, we first compared our Pliocene Productive Series detrital zircon dataset to U/Pb zircon age distributions from the present-day Dnepr, Volga and Don rivers (Wang, Campbell, Stepanov, Allen, & Burtsev, 2011). These two present-day rivers together drain a significant part of the EEC and should therefore be representative for palaeo-sediment provenance from the north. Both samples have a predominance of Late Archean to Proterozoic zircon grains (around 70%), with three significant peaks. The oldest, Late Archean, peak centres around 2.5–2.7 Ga and represents around 10% of the total number of zircons. A second distinct peak is formed by the Palaeoproterozoic (1.6–2.0 Ga), a third during the Mesoproterozoic at 1.0–1.25 Ga. These zircons can be interpreted to have found their origin in the Ukrainian Shield, Fennoscandian and/or Svecofennian orogens and the Sveconorwegian orogeny respectively (Allen et al., 2006). The two rivers differ significantly in their Palaeozoic contribution, where the Volga river contains a large, narrow peak centred around 350 Ma. This is likely related to a contribution to the Volga river sediment from the Ural mountains in the east (Wang et al., 2011), not found in the Don river further to the west.

Jurassic sandstone samples studied by Allen et al. (2006) and Cowgill et al. (2016) from the North Eastern Greater Caucasus, provide limited, but publicly available data to constrain sediment sourcing from this region. The proportions of grain ages from the EEC and Greater Caucasus sources are distinct (Allen et al., 2006; Cowgill et al., 2016). Similar to the Don and Volga samples, the Greater Caucasus source contains zircons with Proterozoic and Archean ages, likely indicating an East European Craton contribution. However, these make up lower contribution from the total sample, with a dominant age range formed by the Palaeozoic and Early Mesozoic grains instead. These must have been sourced from another region, and were interpreted as a local Variscan basement source in the Greater Caucasus region (Allen et al., 2006; Cowgill et al., 2016).

Because of the clear difference between these two source regions, we can compare our Pliocene provenance data in terms of the relative importance of each source area. In our Productive Series sample dataset, we distinguish two different groups of U/Pb zircon ages. The first group consists of samples with predominantly Proterozoic and Archean ages, like Modern Volga, Don or Dnepr. A second group is formed by samples with dominant Mesozoic and Palaeozoic ages (Figure 6). Stratigraphically upwards through the Productive Series, no obvious trend in the detrital zircon age spectra is observed.

Samples from the second group have an important Lower Mesozoic and Palaeozoic contribution, similar to the PS samples analysed by Allen et al. (2006). This seems somewhat less compatible with direct origin from the EEC as none of the present-day northern rivers (Dnepr, Don and Volga) have such contributions. These sediments are known to have been supplied from the north, as indicated by palaeocurrent direction measurements (Hinds et al., 2007). This suggests that north of the Absheron Peninsula a significant contribution of another sediment source entered the Palaeo-Volga delivery system as drainage systems were integrated.

Two potential sediment sources may be identified for the second group. Firstly, the Ural Mountains, sourced through a Palaeo-Ural river. The Ural Mountains have the right age range (with the Main Granite Axis formed between roughly 250 Ma and 330 Ma (Puchkov, 1997). Secondly, the Greater Caucasus may have played an important role as a provenance source. The Group 2 samples show great similarity to the Greater Caucasus Jurassic sandstones, indicating a potential link, with sediments eroding from Greater Caucasus and entering the Pliocene Palaeo-Volga drainage system through Palaeo-Terek

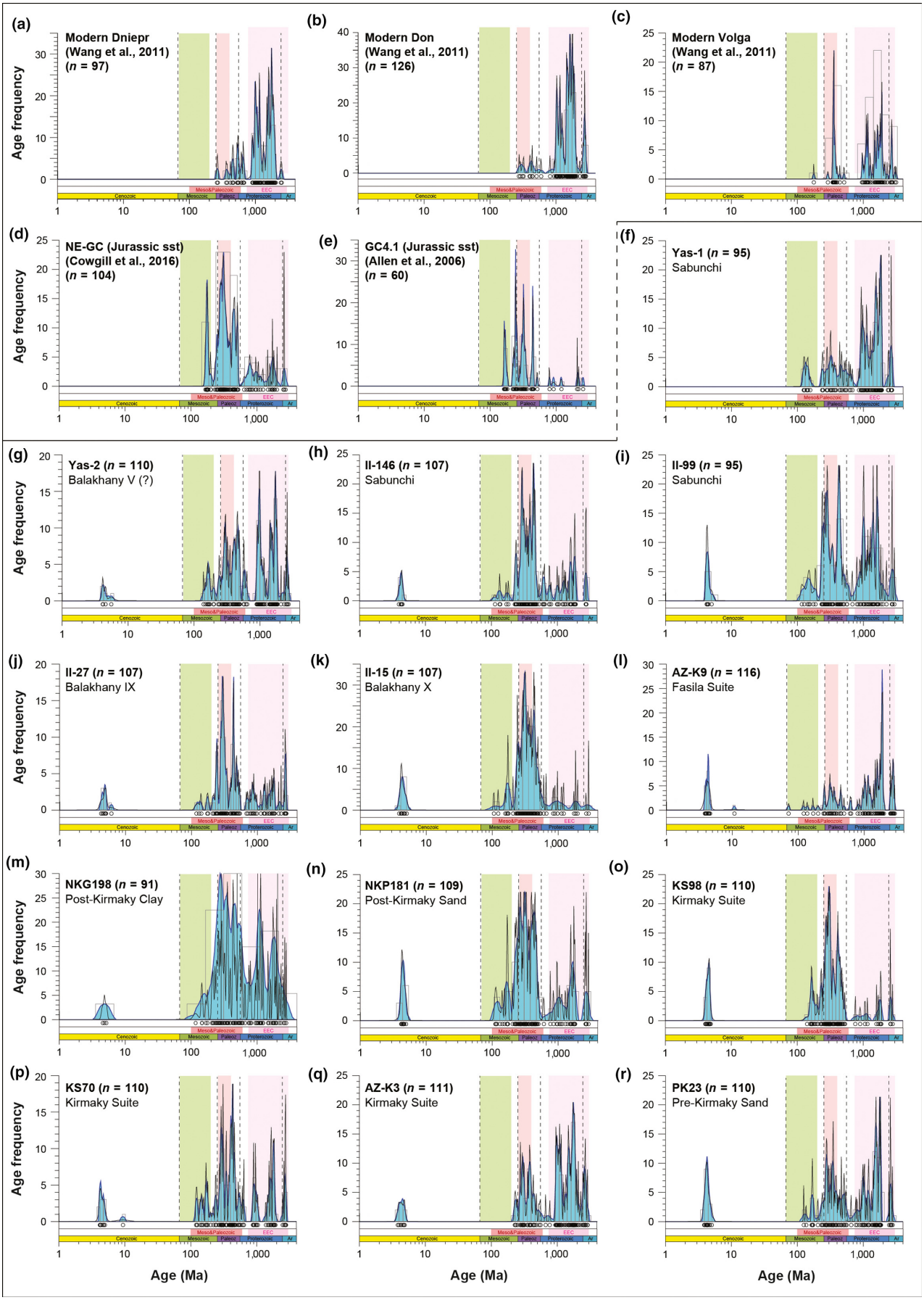
(a)
Modern Dniepr
(Wang et al., 2011)
(n = 97)
(b)
Modern Don
(Wang et al., 2011)
(n = 126)
(c)
Modern Volga
(Wang et al., 2011)
(n = 87)
(d)
NE-GC (Jurassic sst)
(Cowgill et al., 2016)
(n = 104)
(e)
GC4.1 (Jurassic sst)
(Allen et al., 2006)
(n = 60)
(f)
Yas-1 (n = 95)
Sabunchi
(g)
Yas-2 (n = 110)
Balakhany V (?)
(h)
II-146 (n = 107)
Sabunchi
(i)
II-99 (n = 95)
Sabunchi
(j)
II-27 (n = 107)
Balakhany IX
(k)
II-15 (n = 107)
Balakhany X
(l)
AZ-K9 (n = 116)
Fasila Suite
(m)
NKG198 (n = 91)
Post-Kirmaky Clay
(n)
NKP181 (n = 109)
Post-Kirmaky Sand
(o)
KS98 (n = 110)
Kirmaky Suite
(p)
KS70 (n = 110)
Kirmaky Suite
(q)
AZ-K3 (n = 111)
Kirmaky Suite
(r)
PK23 (n = 110)
Pre-Kirmaky Sand
Age frequency
Age (Ma)
Cenozoic
Mesozoic
Paleoz
Proterozoic
Ar
Meso&Paleozoic
EEC

FIGURE 6 Detrital zircon U-Pb ages from the sediment source regions and Productive Series outcrops and an analysis of their provenance implication. (a–c) U/Pb zircon age distributions from the Modern Dniepr, Don and Volga River samples (Wang et al., 2011), where "n" indicates number of grains, (d, e) - U/Pb zircon age distributions from the Jurassic sandstone unit from the North Eastern Greater Caucasus (NE-GC) (Cowgill et al., 2016) and Jurassic sandstone from Greater Caucasus (GC4.1) (Allen et al.,2006), (f–r) - U/Pb zircon age distributions from the Yasamal and Kirmaky Valley samples sorted by stratigraphic position from the youngest in Yasamal valley (f) to the oldest in Kirmaky Valley (r)

branch. There could have been a large degree of reworking of zircon grains throughout Palaeozoic and Mesozoic on EEC and along sediment routing system.

To quantify possible similarities between samples from these two sources, we also calculated likeness between sample populations following the methods of Satkoski, Wilkinson, Hietpas, and Samson (2013). Calculated likeness values are shown in Table 2. These calculations depend on the number of single grain ages per sample. Because our sample size is typically around 100 ages, the maximum theoretical likeness is therefore 72 ± 6%, or 0.72 (Satkoski et al., 2013).

We first used the data from Allen et al. (2006) and Cowgill et al. (2016) in this analysis to show that the Jurassic Sandstone and the modern Volga show low similarity (likeness of 0.266). In general, our Productive Series samples have variable amounts of likeness; sample KS98 has high likeness (0.706) with the NE-GC samples; and sample AZ–K9 has the highest likeness with the Modern Volga samples (0.548).

Most samples have slightly more likeness with NE-GC sample from Cowgill et al. (2016) than with the Modern Volga samples. AZ–K3 (preKirmaky Sand), AZ–K9 (Fasila) and PK–23 sampled from the most massive sandstones in the Productive Series, exhibit a high likeness with the Modern Volga samples, and KS98 (Kirmaky Suite), a sand sample from the middle of a mudstone suite, has the lowest likeness with the Modern Volga samples (Figure 6). This may suggest that throughout deposition of the Productive Series there was always an interplay between a mix of sources, and coarsest clastic intervals were supplied predominantly from the source with signatures most similar to the Modern Volga (i.e. the Palaeo-Volga).

It is also possible that likeness cannot be used as a proxy for sediment provenance because it is distorted by zircon "fertility", with higher amount of zircons generated in volcanic-rich parts of Greater Caucasus, for example, making quantification of provenance area contribution very difficult.

5.1.3 | "Young" grain group and maximum depositional ages

Our "young" grain group consisted of grains with Pliocene and late Miocene ages that are important for establishing new constraints on depositional ages and sedimentation rates. Because the ages of these "young" grains match those of the main volcanic events in the Lesser Caucasus (Dilek, Imamverdiyev, & Atunkaynak, 2010; Westaway, 1994), we interpret them to be the result of volcanic ash falls sourced in the Lesser Caucasus or Talesh Mountains, mixing with Productive Series sands during transit into the South Caspian Basin.

The distribution of measured ages in all of the Neogene grains is shown in Table 3 that contains 99 ages from 13 samples. In this dataset, one detrital zircon age is considered an outlier due to its large error—the 10.75 ± 6.24 Ma age from sample 2011—AZ–K9. Excluding this single datum, the oldest Neogene grain has an age of 5.55 ± 0.59 Ma (Yas–1), and the youngest has an age of 3.84 ± 0.28 Ma (2011–AZ–K9). As discussed in the previous section, we present maximum depositional ages as: (i) the youngest single grain age, (ii) the pooled average age and (iii) the weighted mean age for the sample cluster that overlaps with the single youngest grain at 2σ (Table 3). Weighted-mean ages were calculated using the AGEPICK program as described in Dickinson and Gehrels (2009).

In analysing our data set, we have been guided by one key principle that helped us constrain maximum

TABLE 2 Calculated likeness of Productive Series U/Pb age distributions with two potential source areas, Jurassic sandstone in the Greater Caucasus (after Cowgill et al., 2016) and the Modern Volga (after Wang et al., 2011). Stratigraphic levels positions are on Figure4

Sample Name	Stratigraphy	Jurassic sst (NE-GC)	Modern Volga
NE-GC	Jurassic sst	1	0.266
Yas-1	Sabunchi	0.346	0.502
Yas-2	Balakhany VI	0.518	0.402
II-146	Sabunchi	0.626	0.329
II-99	Balakhany V	0.531	0.36
II-27	Balakhany VIII	0.619	0.292
II-15	Balakhany IX	0.67	0.254
AZ-K9	Fasila	0.395	0.548
NKG198	NKG	0.548	0.403
NKP181	NKP	0.632	0.312
KS98	Kirmaky Suite	0.706	0.237
KS70	Kirmaky Suite	0.537	0.346
AZ-K3	PreKirmaky	0.422	0.571
PK23	PreKirmaky	0.519	0.436
Modern Volga		0.266	1

depositional ages. The key principle for defining a maximum depositional age is that the sandstones from which the samples were taken must be younger or of similar age to our "young" zircon grains.

A first observation was that there is considerable age range overlap in all the "young" samples. It was therefore not possible to distinguish separate events—in our case assumed specific Pliocene volcanic ash falls—that led to particular ages. Secondly, no trend was observed in weighted mean ages from the data set (Figure 5). If anything, weighted mean ages of Sabunchy or Surakhany Suite samples are older than weighted mean ages of PK and Kirmaky Suite samples suggesting a possible random distribution of volcanic grains (Table 2). The events (probable Pliocene volcanic ash falls) that lead to the existence and presence of these young grains are evident in almost all the samples we analysed and must have been persistent and continuous throughout Productive Series deposition, peaking at 4 Ma, or after. Since the ages of the Pliocene volcanic air fall grains do not show a consistent trend at least some of the zircon grains are reworked rather than being derived directly.

For the determination of the maximum depositional ages, grains of most interest and importance are the ones that give youngest ages for the oldest stratigraphic unit. Analysing weighted mean average ages (our preferred method) we found the two most useful samples to date: Productive Series: (i) a sample taken from the PK suite (PK–23) with the youngest single grain age of 3.89 ± 0.3 Ma and weighted mean age of 4.0 ± 0.1 Ma and (ii) the next closest sample from the Kirmaky suite (2011–AZ–K3) that also gave youngest single grain age of 3.86 ± 0.36 Ma and weighted mean of 4.0 ± 0.1 Ma (Table 3). All other maximum depositional ages were derived from stratigraphically younger samples and yielded detrital zircon ages older than the youngest preferred weighted mean average age of PK–23. They, therefore, do not provide additional geochronological information. There were 11 grains with single ages younger than our weighted mean age for PK–23 of 4.0 Myr (shown by bold italics in Table 3). They are present in PK–23 (two ages in PK), 2011–AZ–K3 (two ages in Kirmaky), 2011–AZ–K9 (four ages in Fasila), II–15 (one age in Balakhany) and II–146 (two ages in Sabunchy). However, there is no consistent distribution of these single grain ages throughout the section.

Our preferred method for quantifying maximum depositional ages for subunits in the Productive Series is method (d) of Dickinson and Gehrels (2009)—using the mean age of the youngest three or more grains that overlap in age at 2σ (Table 3). This method is the most statistically robust and gives conservative ages when compared to individual youngest grains, and gave a robust weighted mean age of 4.0 ± 0.1 Ma for the age of PK suite. This result is based on an average sample of around 100 single-grain Neogene ages, being the largest sample set to date (Table 3). With the ongoing trend in U/Pb detrital zircon age studies to use increasingly larger numbers (>1,000) of single grain ages per sample (e.g. Pullen, Gehrels, Ibanez-Mejia, & Pecha, 2014), future larger sample set sizes will likely result in older average ages. If these hypothetical future studies were conducted to accumulate a large (>1,000 samples) distribution of Neogene age U/Pb samples, they might be expected to find older statistically defined maximum depositional ages than we have here.

5.2 | Apatite (U–Th–Sm)/He

Apatite (U–Th–Sm)/He geochronology was undertaken on 57 grain ages acquired from 12 Kirmaky and Yasamal Valley samples (Table 4). Significantly, fewer apatite grains per sample were analysed compared to the larger numbers of detrital zircon grains analysed. Out of these 57 samples, 28 gave Neogene ages (49%), and the rest gave Palaeogene (18%), Mesozoic (26%), Palaeozoic (8%) or gave no meaningful ages (Figure 7). The absence of Palaeozoic and Proterozoic samples may be a reflection of (i) the poorer durability of apatite grains (compared to that of zircon grains), or (ii) the fact that the (U–Th–Sm)/He apatite grain ages reflect exhumation and cooling through low near surface (~75°C) temperatures. Our apatite (U–Th–Sm)/He results created a new and unexpected focus for this study.

Stratal patterns and high (primary?) sandstone porosity both suggest that the Productive Series strata we studied exposed in the cores of the two South Caspian anticlines was never deeply buried and that these anticlines were growing in amplitude during post-Productive Series deposition. Only a thin cover of Pleistocene (Absheronian) growth strata exists on the anticlinal crests, and it thickens considerable into the troughs (e.g. Baku Bay) between the anticlines. In addition, sandstone beds in the Productive Series are world-class reservoir rocks that typically have (primary) porosity values of ~20% or greater. We thus interpret that apatite (U-Th-Sm)/He ages were not reset following deposition of Productive Series. Time–temperature curves could not be constructed for the rocks exposed in the cores of the Yasamal and Kirmaky anticlines as we had set out to do, and subsequently, the exhumation histories of these macrofolds could not be determined. The exhumation ages of the apatite grains should provide clues as to where these sand grains were exhumed and sourced from, as well as the maximum age of their host (i.e. Productive Series) sediment. However, a paucity of samples and relatively high proportion of grains with Neogene ages, which constitute almost half of the sample set (Table 4; Figure 7) render detailed provenance studies difficult. The apatite

TABLE 3 zircon grain U/Pb age data from the "youngest" Neogene sample group sorted by formation

Sample number	Stratigraphy	Sample name	Preferred single grain (Ma)	Error (−2σ)	Error (+2σ)	Youngest Age (Ma)	Oldest Age (Ma)	Averaged age of selected grains (Ma)	Weighted mean averaged age of selected samples with error using AGEPICK (Ma)	U, ppm	Th, ppm	U/TH
1	Kirmaky/PK	PK23	***3.888***	***0.28***	***0.28***	***3.61***	***4.16***	3.97	4.00 ± 0.1	**590**	**219**	**2.7**
			3.91	***0.27***	***0.27***	***3.64***	***4.19***			**588**	**218**	**2.7**
			3.94	***0.48***	***0.48***	***3.47***	***4.42***			**487**	**195**	**2.5**
			4.12	*0.18*	*0.18*	*3.94*	*4.30*			1,977	1,397	1.4
			4.20	0.20	0.20	4.00	4.40			2,827	220	12.8
			4.23	0.64	0.64	3.59	4.87			433	185	2.3
			4.29	0.21	0.21	4.09	4.50			2,346	484	4.8
			4.32	0.64	0.64	3.68	4.96			433	185	2.3
			4.34	0.20	0.20	4.14	4.54			2,016	121	16.7
			4.44	0.41	0.41	4.02	4.85			3,328	3,287	1.0
			4.49	0.56	0.56	3.93	5.06			848	663	1.3
			4.69	0.85	0.85	3.84	5.54			192	80	2.4
			4.72	0.39	0.39	4.33	5.11			467	233	2.0
			5.05	0.47	0.47	4.58	5.52			521	150	3.5
2	Kirmaky	2011-AZ-K3	***3.86***	***0.36***	***0.36***	***3.50***	***4.22***	3.92	4.00 ± 0.2	**792**	**378**	**2.1**
			3.98	***0.3***	***0.3***	***3.68***	***4.28***			**3,249**	**3,984**	**0.8**
			4.23	0.47	0.47	3.76	4.70			792	204	3.9
			4.34	0.38	0.38	3.96	4.72			592	221	2.7
			4.59	0.57	0.57	4.02	5.16			733	301	2.4
			4.74	0.55	0.55	4.19	5.29			891	465	1.9
			4.87	0.23	0.23	4.64	5.10			5,541	580	9.6
3	Kirmaky	KS70	*4.18*	*0.25*	*0.26*	*3.92*	*4.43*	4.24	4.30 ± 0.2	1,112	450	2.5
			4.19	*0.44*	*0.44*	*3.75*	*4.63*			468	128	3.7
			4.28	*0.64*	*0.64*	*3.64*	*4.92*			433	185	2.3
			4.31	*0.26*	*0.26*	*4.05*	*4.57*			1,804	251	7.2
			4.52	0.45	0.45	4.07	4.98			277	68	4.0
			4.74	0.67	0.67	4.07	5.41			308	75	4.1
			4.76	0.41	0.41	4.36	5.17			465	232	2.0
			4.98	0.51	0.51	4.47	5.49			392	131	3.0

(Continues)

TABLE 3 (Continued)

Sample number	Stratigraphy	Sample name	Preferred single grain (Ma)	Error (−2σ)	Error (+2σ)	Youngest Age (Ma)	Oldest Age (Ma)	Averaged age of selected grains (Ma)	Weighted mean averaged age of selected samples with error using AGEPICK (Ma)	U, ppm	Th, ppm	U/TH
4	Kirmaky	KS98	*4.04*	*0.35*	*0.35*	*3.70*	*4.39*	4.22	4.20 ± 0.1	946	585	1.6
			4.11	*0.41*	*0.41*	*3.70*	*4.52*			980	418	2.3
			4.16	*0.29*	*0.29*	*3.87*	*4.44*			1,111	966	1.2
			4.26	*0.21*	*0.21*	*4.05*	*4.47*			2,358	491	4.8
			4.33	*0.33*	*0.33*	*4.00*	*4.67*			1,240	1,065	1.2
			4.40	*0.16*	*0.16*	*4.24*	*4.56*			3,533	1,959	1.8
			4.52	0.41	0.41	4.11	4.94			617	170	3.6
			4.54	0.31	0.31	4.23	4.85			2,928	734	4.0
			4.58	0.14	0.15	4.43	4.72			7,556	869	8.7
			4.61	0.16	0.16	4.45	4.76			9,270	816	11.4
			4.73	0.36	0.35	4.37	5.08			1,010	267	3.8
			4.74	0.18	0.18	4.56	4.93			7,832	10,493	0.7
			4.85	0.57	0.57	4.28	5.42			449	120	3.8
5	Nad-Kirmaky (NKP)	NKP181	*4.17*	*0.73*	*0.73*	*3.43*	*4.90*	4.44	4.4 ± 0.1	415	82	5.1
			4.28	*0.23*	*0.23*	*4.05*	*4.51*			1,303	681	1.9
			4.31	*0.22*	*0.22*	*4.09*	*4.52*			2,363	495	4.8
			4.44	*0.43*	*0.43*	*4.01*	*4.86*			3,333	3,327	1.0
			4.52	*0.45*	*0.45*	*4.07*	*4.97*			601	275	2.2
			4.54	*0.68*	*0.68*	*3.86*	*5.22*			364	150	2.4
			4.59	*0.56*	*0.56*	*4.03*	*5.15*			816	624	1.3
			4.65	*0.69*	*0.69*	*3.96*	*5.33*			342	110	3.1
			4.98	0.38	0.39	4.59	5.36			743	228	3.3
6	Nad-Kirmaky (NKG)	NKG198	*4.55*	*0.34*	*0.35*	*4.21*	*4.90*	4.71	4.80 ± 0.2	1,722	389	4.4
			4.86	*0.25*	*0.25*	*4.61*	*5.11*			1,890	296	6.4
			5.19	*0.35*	*0.35*	*4.84*	*5.54*			2,254	162	13.9
7	Fasila	2011-AZ-K9	***3.84***	***0.55***	***0.55***	***3.29***	***4.39***	4.13	4.1 ± 0.1	**608**	**288**	**2.1**
			3.87	***0.48***	***0.48***	***3.39***	***4.35***			**1,238**	**844**	**1.5**
			3.94	***0.46***	***0.46***	***3.48***	***4.40***			**936**	**431**	**2.2**
			3.98	***0.46***	***0.46***	***3.52***	***4.44***			**942**	**439**	**2.1**

(Continues)

TABLE 3 (Continued)

Sample number	Stratigraphy	Sample name	Preferred single grain (Ma)	Error (−2σ)	Error (+2σ)	Youngest Age (Ma)	Oldest Age (Ma)	Averaged age of selected grains (Ma)	Weighted mean averaged age of selected samples with error using AGEPICK (Ma)	U, ppm	Th, ppm	U/TH
			4.08	*0.73*	*0.73*	*3.35*	*4.81*			803	326	2.5
			4.11	*0.36*	*0.36*	*3.75*	*4.47*			1,801	984	1.8
			4.12	*0.34*	*0.34*	*3.78*	*4.46*			1,525	1,068	1.4
			4.29	*0.56*	*0.55*	*3.73*	*4.84*			639	335	1.9
			4.3	*0.47*	*0.47*	*3.83*	*4.77*			1,174	484	2.4
			4.32	*0.91*	*0.91*	*3.41*	*5.23*			807	336	2.4
			4.35	*0.69*	*0.69*	*3.66*	*5.04*			1,133	488	2.3
			4.39	*0.46*	*0.46*	*3.93*	*4.85*			1,164	775	1.5
			4.48	0.38	0.38	4.10	4.86			2,343	2,308	1.0
			4.61	0.27	0.27	4.34	4.88			808	360	2.2
			10.75	6.24	6.22	4.51	16.97			1,273	532	2.4
8	Balakhany IX	II-15	***3.89***	*0.28*	*0.28*	*3.61*	*4.17*	4.06	4.1 ± 0.1	588	219	2.7
			4.14	*0.30*	*0.29*	*3.85*	*4.44*			1,120	631	1.8
			4.15	*0.19*	*0.18*	*3.96*	*4.33*			1,952	1,368	1.4
			4.22	0.21	0.21	4.01	4.43			2,834	221	12.8
			4.32	0.20	0.20	4.12	4.52			2,016	121	16.6
			4.52	0.25	0.25	4.26	4.77			1,865	824	2.3
			4.65	0.85	0.85	3.80	5.50			192	80	2.4
			4.74	0.42	0.42	4.32	5.17			466	232	2.0
			5.03	0.45	0.45	4.58	5.47			518	150	3.5
9	Balakhany VIII	II-27	*4.28*	*0.49*	*0.49*	*3.79*	*4.77*	4.46	4.4 ± 0.4	757	351	2.2
			4.47	*0.63*	*0.63*	*3.84*	*5.11*			436	372	1.2
			4.63	*1.04*	*1.04*	*3.59*	*5.67*			346	270	1.3
			4.86	0.42	0.42	4.44	5.28			1,289	191	6.8
			4.95	0.39	0.39	4.55	5.34			1,555	123	12.7
			5.06	0.33	0.33	4.73	5.39			1,232	132	9.3
10	Sabunchy	II-99	*4.23*	*0.24*	*0.24*	*3.99*	*4.48*	4.32	4.3 ± 0.1	987	163	6.1
			4.24	*0.24*	*0.24*	*4.00*	*4.48*			987	163	6.0
			4.27	*0.24*	*0.24*	*4.03*	*4.51*			1,178	73	16.1

(Continues)

TABLE 3 (Continued)

Sample number	Stratigraphy	Sample name	Preferred single grain (Ma)	Error (−2σ)	Error (+2σ)	Youngest Age (Ma)	Oldest Age (Ma)	Averaged age of selected grains (Ma)	Weighted mean averaged age of selected samples with error using AGEPICK (Ma)	U, ppm	Th, ppm	U/TH
			4.37	*0.24*	*0.24*	*4.13*	*4.61*			838	40	20.9
			4.46	*0.49*	*0.49*	*3.98*	*4.95*			195	78	2.5
			5.00	0.57	0.57	4.43	5.56			213	49	4.3
11	Sabunchy	II-146	*3.96*	*0.27*	*0.27*	*3.69*	*4.24*	4.08	4.1 ± 0.2	588	218	2.7
			4.21	*0.47*	*0.47*	*3.74*	*4.67*			952	548	1.7
			4.31	0.64	0.64	3.67	4.95			433	185	2.3
			4.35	0.16	0.16	4.19	4.51			3,533	1,959	1.8
			4.49	0.41	0.41	4.08	4.91			617	170	3.6
13	Surakhany	Yas-2	*4.14*	*0.44*	*0.44*	*3.70*	*4.58*	4.29	4.3 ± 0.2	468	128	3.7
			4.16	*0.19*	*0.18*	*3.97*	*4.34*			1,952	1,368	1.4
			4.57	*0.25*	*0.25*	*4.31*	*4.82*			1,865	824	2.3
			5.55	1.18	1.18	4.37	6.73			256	102	2.5

Italic font designates grains with ages overlap at 2σ. Bold font shows where ages are younger than 4.0 Myr.

TABLE 4 Apatite (U–Th–Sm)/He grain ages count from Kirmay and Yasamal outcrop samples

Sample name Formation	AZK5 KS	AZK10 KS	AZK11 Bal	AZK6 KS	AZK7 NKP	AZK8 NKG	AZY1 Bal	AZY2 Bal	AZY3 Sabunchy	AZY6 Sabunchy	AZY7a Sabunchy	AZY7b Sab/Sur	Total number of samples	Percentage of total
Neogene	2	3	2	2	1	4	2	2	1	1	5	3	28	49.1
Palaeogene	0	0	1	2	1	1	1	2	1	0	0	0	9	15.8
Mesozoic	3	1	1	1	2	0	1	1	1	1	0	0	12	21.1
Palaeozoic	2	0	0	1	1	1	0	0	0	0	0	0	5	8.8
Proterozoic	0	0	0	0	0	0	0	0	0	0	0	0	0	0.0
Archean	0	0	0	0	0	0	0	0	0	0	0	0	0	0.0
Total	7	4	4	6	5	6	4	5	3	2	5	3	57	

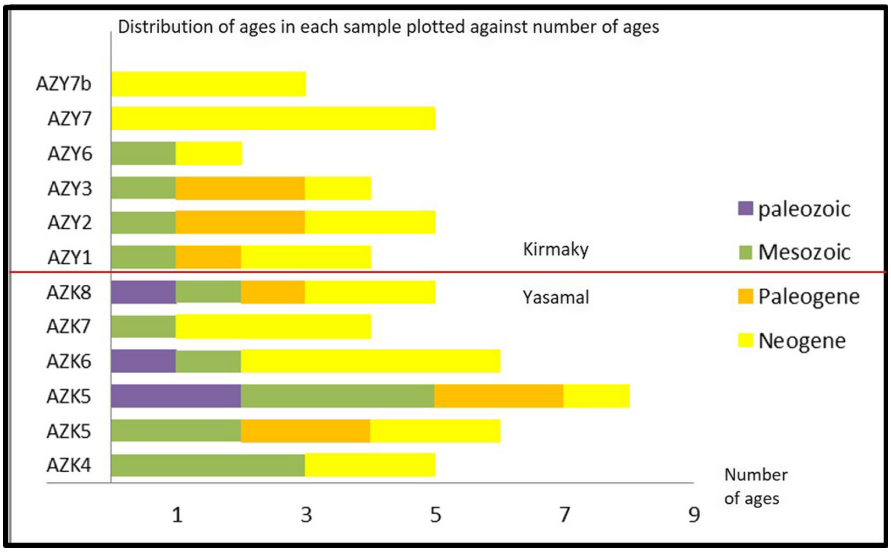

FIGURE 7 Detrital apatite (U-Th-Sm)/He chart showing distribution of the grain ages on samples from the oldest stratigraphic unit (AZK-4) at Kirmaky Trench to the youngest in Yasamal valley (AZY7b)

(U-Th-Sm)/He method, however can be used as complementary method to determine maximum depositional ages for Productive Series subunits.

Table 5 shows the (U–Th–Sm)/He apatite ages for the 28 Neogene age samples. The methods of Dickinson and Gehrels (2009) were again applied to calculate maximum depositional ages. Because there were only few Neogene age grains, and most had no 2σ age overlaps, only one single grain age from sample AZK6 (Kirmaky Valley; preferred age of 3.0 ± 0.18 Ma) and two single grains from sample AZY7b [Yasamal Valley; preferred weighted mean age of 2.9 ± 0.2 Ma, using Dickinson and Gehrels' (2009) method (d), outlined above] were available to compare to and supplement our detrital zircon ages. Sample AZY7b nearly had a sufficient 2σ overlap for the three youngest grains to be used to determine maximum depositional ages for Productive Series subunits; using all three grains which do not quite overlap at 2 s would give a weighted mean age of 3.3 ± 0.2 Ma. All other ages obtained were older than the <5.38 Myr age constraint from the underlying Pontian (van Baak et al., 2016), and/or had no overlaps at 2σ, so were therefore excluded. Even though there is a statistically much smaller sample set of Neogene detrital apatite grains compared to zircon (28 vs. 109), some of the ages provided by apatite (U–Th–Sm)/He geochronology can potentially be used. An integrated interpretation of the findings is explored and a new timescale is proposed in our conclusions section below.

5.3 | Productive Series age models and South Caspian Basin sedimentation rate calculations

Information from the detrital zircon U/Pb supplemented by apatite grain (U–Th–Sm)/He ages allows for better constraint of the Productive Series maximum depositional age. In this study, we first constructed an age model using only detrital zircon U/Pb ages. As an alternative we then discuss how to apply our supplemental apatite grain (U–Th–Sm)/He ages in creating an alternative age model.

The age models were further constrained at the base by a maximum age of 5.38 Ma, representing the youngest known deposition of the underlying Pontian stage (van Baak et al., 2016). At the top, the age models were constrained at 2.71 Ma, the age of the base of the overlying Akchagyl stage (van Baak, 2015).

Using U/Pb zircon maximum deposition age analysis (section 5.1), we found that the most critical sample for dating the Productive Series was from the PK suite (PK–23) with the youngest single grain age of 3.89 ± 0.28 Ma and weighted mean age of 4.0 ± 0.1 Ma. The second most critical was sample 2011–AZ–K3 that had a youngest single grain age of 3.89 ± 0.36 Ma and a weighted mean of 4.0 ± 0.1 Ma. All other maximum depositional ages were from stratigraphically younger samples and yielded detrital ages older than or similar to the youngest mean age of PK–23. Therefore, we used only these two dates to constrain our new timescale and sedimentation rates for the Productive Series (Figure 8).

Using the schematic stratigraphy from Azizbekov (1972), Aliyev (1949), Hinds et al. (2007) and Salmanov et al. (2015), thickness of the Pliocene Productive Series exposed in various outcrops above the PK suite assumed at ~1.7 km in (Figure 3). Green et al. (2009) and Abdullayev et al. (2012), using well log correlation, seismic reflection mapping and isopach determinations, showed that the thickness of the Productive Series increases to >5 km offshore South Caspian Basin. Below the PK, an interval belonging to the Qala Suite is also present offshore but not exposed anywhere onshore in Azerbaijan, thickness of Qala suite from seismic data reaches 1 km (Green et al., 2009).

TABLE 5 Apatite (U–Th–Sm)/He grain ages sorted by formation

Sample number	Stratigraphy	Sample name	Weighted mean averaged age of selected samples with error using AGEPICK (Ma)	Preferred age (Ma)	Error (−2σ)	Error (+2σ)	Youngest age (Ma)	Oldest age (Ma)
1	Kirmaky	AZK5	4.3	4.3	0.52	0.52	3.78	4.82
				14	1.68	1.68	12.32	15.68
2	Kirmaky	AZK6	3.0	3	0.36	0.36	2.64	3.36
				12.6	1.5	1.5	11.1	14.1
5	Kirmaky?	AZK10	4.7	4.7	0.56	0.56	4.14	5.26
		AZK10		9.3	1.12	1.12	8.18	10.42
		AZK10		16.8	2.02	2.02	14.78	18.82
3	NKP	AZK7	13.7	13.7	1.64	1.64	12.06	15.34
4	NKG	AZK8	9.5	9.5	1.14	1.14	8.36	10.64
		AZK8		14.2	1.7	1.7	12.5	15.9
		AZK8		20.7	2.48	2.48	18.22	23.18
		AZK8		22.2	2.66	2.66	19.54	24.86
6	Balakhany?	AZK11	6.2	6.2	0.74	0.74	5.46	6.94
		AZK11		22.6	2.72	2.72	19.88	25.32
7	Balakhany	AZY1	6.4	6.4	0.76	0.76	5.64	7.16
		AZY1		14.5	1.74	1.74	12.76	16.24
8	Balakhany	AZY2	3.7	3.7	0.44	0.44	3.26	4.14
		AZY2		8.9	1.06	1.06	7.84	9.96
9	Balakhany	AZY3	13	13	1.56	1.56	11.44	14.56
		AZY6		14.2	1.7	1.7	12.5	15.9
10	Sabunchy?	AZY7A	10.8	10.8	1.3	1.3	9.5	12.1
		AZY7A		11.3	1.36	1.36	9.94	12.66
		AZY7A		13.4	1.62	1.62	11.78	15.02
		AZY7A		15.3	1.84	1.84	13.46	17.14
		AZY7A		15.9	1.9	1.9	14	17.8
11	Sabunchy/ Surakhany	AZY7b	3.3	*2.9*	*0.34*	*0.34*	*2.56*	*3.24*
		AZY7b		*2.9*	*0.34*	*0.34*	*2.56*	*3.24*
		AZY7b		*4*	*0.48*	*0.48*	*3.52*	*4.48*

Italic font designates grains whose ages overlap at 2σ.

The Qala Suite sits on top of what is interpreted as a major base-level fall unconformity (Abdullayev et al., 2012; Reynolds et al., 1998).

Using these thickness estimates allowed us to provide sedimentation rates for key Productive Series subunits. In our tentative age model (Figure 8), the 4.0 ± 0.1 Myr U/Pb detrital zircon age from PK divides the Productive Series in to two approximately equal time intervals. The duration of the Qala Suite is estimated at a maximum of 1.38 Myr and duration of interval from PK to Top Productive Series is ~1.3 Myr. Sedimentation rates for the offshore Qala Suite are in the order of 0.72 km/Myr. Between the PK and the top of the Productive Series, sedimentation rate increases to 1.3 km/Myr at outcrop and to 3.9 km/Myr in the centre of the offshore basin (Table 6). These are among the highest sedimentation rates ever reported for a large sedimentary basin, equalling or exceeding sediment accumulation rates reported for the Bengal Fan in Pliocene (Metivier, Gaudemer, Tapponnier, & Klein, 1999) and the Amazon Fan in Quaternary (Figueiredo, Hoorn, van Der Ven, & Soares, 2009), reported on average at 1.1 km/Myr and 1.22 km/Myr respectively.

Supplementing the results from detrital zircon U/Pb by detrital apatite (U–Th–Sm)/He weighted mean grain ages (Figure 8) from the only relevant sample AzY7b (Sabunchy) may further subdivide Productive Series intervals into two further subunits. First subunit between PK and Sabunchy will have a duration between 4.0 Myr to 3.3 Myr and

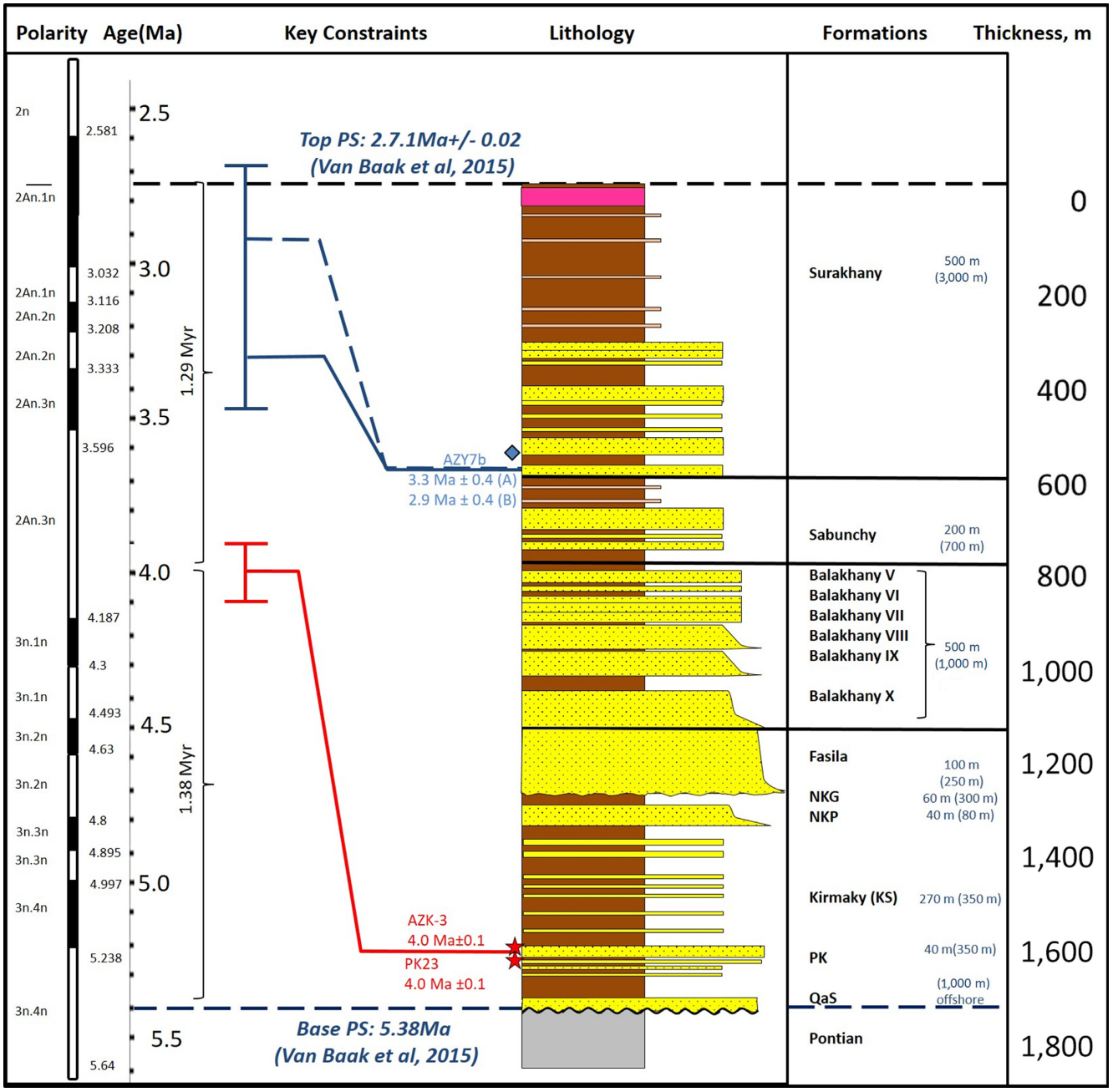

FIGURE 8 Tentative Productive Series timescale based on Zircon U-Pb constraints supplemented by detrital apatite (U-Th-Sm)/He constraints. Maximum depositional ages for relevant samples provide the youngest age in the lowest stratigraphic position based on and are method (d) from Dickinson & Gehrels, 2009 (shown in red stars). For comparison we show also show palaeomagnetic timescale from Hilgen et al. (2012)

onshore sedimentation rate of 1.02 km/Myr. Second sub \unit between Sabunchy and Top Productive Series will have a duration between 3.3 Ma to 2.71 Myr and onshore sedimentation rates of 3.55 km/Myr (Table 6). We also observed that two apatite (U–Th–Sm)/He ages from the Yasamal Valley (sample AZY–7b) had similar preferred age of 2.9 Myr which, if true, will have even more drastic effect on sedimentation rates. However, the current paucity of young apatite grain ages when compared with those from our robust detrital zircon U/Pb data set does not allow us to build a very confident age model using either of the possible AZY-7b apatite (U-Th-Sm)/He ages. The age model on Figure 8 is plotted in comparison to recent Global Polarity Time Scale (Hilgen et al., 2012), but has not been modified to accommodate existing palaeomagnetic measurements in van Baak et al. (2016) due to their incompleteness.

Irrespective of the method used in calculating of maximum depositional ages, the sedimentation rates we derive are dramatically large in magnitude when compared with

TABLE 6 Age model and sedimentation rate for Pliocene Productive Series using Zr U-Pb age constraints, supplemented by Apatite (U–Th–Sm/He) ages

Sedimentation rate locations	Timescale (Zr U-Pb only)					Timescale (Zr U/Pb and apatite (U–Th–Sm)/He)				
	Stratigraphy	Thickness (km)	Age (Ma)	Duration (Ma)	Sedimentation Rate (km/Ma)	Stratigraphy	Thickness (km)	Age (Ma)	Duration (Ma)	Sedimentation rate (km/Ma)
Onshore (outcrops)	Middle-Upper PS	1.7	4.0–2.71	1.29	1.32	PK to Top Sabunchy	0.6	4.0–3.3	0.59	1.02
						Top Sabunchy to Top PS	1.1	3.3–2.71	0.3	3.55
Offshore Average	Lower PS (Qala/PK)	1	5.38–4.0	1.38	0.72	Lower PS (Qala/PK)	1	5.38–4.0	1.38	0.72
						PK to Top Sabunchy	2.35	4.0–3.3	0.7	3.4
	Middle-Upper PS (PK to Top PS)	5	4.0–2.71	1.29	3.88	Top Sabunchy to Top PS	3.35	3.3–2.71	0.59	5.7

those from other sedimentary basins. The timing of this drastic increase in sedimentation rate after 4 Ma may coincide with a similar increase around the globe at 2–4 Myr in a variety of settings, including active and inactive mountain belts and inland basins that are not affected by sea-level changes (Hay, Sloan, & Wold, 1988; Zhang, Molnar, & Downs, 2001). These global observations of increased sedimentation, and of coarser material since 5 Myr suggest a possible cause by a climate shift, from relatively stable and unvarying climate to the one changing rapidly via Milankovitch forcing, with frequent and abrupt changes in temperature, precipitation and vegetation, and with erosive processes dominant (Molnar, 2004; Zhang et al., 2001).

The observed post-4 Ma increase in sedimentation rates in the Pliocene Productive Series may coincide with such a shift, but is probably significantly amplified by isolation of the South Caspian Basin after 5.38 Ma. The observation of young apatite ages of approximately 3 Myr (Sabunchy sample AZY7b) could signal even more rapid sedimentation rates in the Upper Productive Series, coincident with global cooling, onset of northern hemisphere glaciation and a shift to high-amplitude oscillations dominated by the 100,000-year period of the orbital eccentricity (Zhang et al., 2001).

Further work should focus on improving detrital zircon and apatite grain data sets by obtaining more densely spaced samples with larger sample size to better constrain absolute ages and sedimentation rates in the Productive Series at both Kirmaky and Yasamal Valleys, and any additional outcrops that can be sampled. Integration of detailed magnetostratigraphy, modelling climatically driven Milankovtich cycles, cyclostratigraphy studies of the whole Productive Series as well as age dating of the Pontian formations at the Kirmaky Valley outcrops, is also recommended to produce a more consistent time scale for all of the Productive Series units.

6 | CONCLUSIONS

The age of the Pliocene Productive Series, Azerbaijan—a major deposit in the South Caspian Basin, had not been well constrained previously due to the absence of adequate biostratigraphic control. It had been generally thought that Productive Series represents an unusually rapid period of clastic deposition in this inland basin and that it was sourced from the European Craton and Greater Caucasus. However, the onset of deposition and accurate calculations of sedimentation rates within the Productive Series were difficult without solid internal age constraints. In addition, the provenance of the Pliocene Productive Series had not been well constrained.

In this study, we used detrital zircon U/Pb geochronology supplemented by (U–Th–Sm)/He geochronology to better define the deposition and constrain provenance of the Productive Series. U/Pb analysis of detrital zircon grains from Productive Series sandstone outcrops in the Kirmaky and Yasamal Valleys, Absheron Peninsula, Azerbaijan, produced two distinct families of grains—"young" Neogene grains and "old" Mesozoic, Palaeozoic and Proterozoic grains. We compared the "old" grain ages with known Modern Volga and Greater Caucasus sandstone detrital U/Pb zircon age distributions to better understand the sediment source areas of the Pliocene Productive Series. Our observations support previous provenance studies which suggested that the Productive Series shows an affinity for both the Greater Caucasus and the Modern Volga (East European Craton) sources. Our study indicates a slightly higher similarity with a Greater Caucasus source than a Volga source, and confirms a mix of these two provenance sources. Some Productive Series sandstone intervals (PK suite and Fasila Suite) show Zircon U/Pb age distributions that are more similar to the Modern Volga, suggesting increase in relatively contribution from palaeo-Volga (East European Craton) source in these massive sandstones.

We interpret the "young" Neogene zircon grains likely resulted from contemporaneous volcanic air falls sourced from the Lesser Caucasus or Talesh Mountains. A dataset of 100 Neogene age grains, collected from over 13 samples, provides new maximum depositional age constraints for the deposition of the Lower Productive Series. This indicates that the oldest sediments exposed in outcrop (PK Suite) were deposited around 4.0 Ma, much earlier than previously suspected. Previous work had constrained the age of the base and top of the Productive Series. Our maximum deposition age of around 4.0 Ma for the PK Suite provides a crucial tie-point within the Productive Series succession. This tie-point divides the entire Productive Series time interval into two parts of near-equal duration. The lower part, the Qala Suite, was deposited offshore with a sedimentation rate of ~0.7 km/Myr. A large increase in sedimentation rate occurred ~4.0 Ma around the base of the PK Suite with the majority of the Productive Series (base PK–top PS) deposited at the rate of 1.3 km/Myr onshore Absheron peninsula and up to a maximum of 3.9 km/Myr offshore South Caspian. These sedimentation rates are among the highest reported for sedimentary basin and are comparable to those in major modern high-volume sediment fairways, such as Bengal fan or Amazon fan. The increase in sedimentation rates may coincide with a global increase in sedimentation rates after 4 Myr and could be related to a global climatic shift, amplified by the isolation of the South Caspian Basin and the enhanced integration of river drainage systems supplying sediment into it.

The (U–Th–Sm)/He geochronology method may provide some additional constraints for the ages of Pliocene Productive Series, but the paucity of apatite grains suggest a need for more thorough sampling before these data can be accurately integrated into a Productive Series timescale.

ACKNOWLEDGEMENTS

The authors would like to thank Nathan Niemi and Steve Vincent for reviewing the paper and BP for permission to publish the data.

REFERENCES

Abdullayev, N. R. (2000). Seismic stratigraphy of the Upper Pliocene and Quaternary deposits in the South Caspian Basin. *Journal of Petroleum Science and Engineering*, *28*, 207–226. https://doi.org/10.1016/S0920-4105(00)00079-6

Abdullayev, N. R., Kadirov, F., & Guliyev, I. S. (2015). Subsidence history and basin-fill evolution in the South Caspian Basin from geophysical mapping, flexural backstripping, forward lithospheric modelling and gravity modelling. *Geological Society, London, Special Publications*, *427*, SP427–5.

Abdullayev, E., & Leroy, S. A. (2016). Provenance of clay minerals in the sediments from the Pliocene Productive Series, western South Caspian Basin. *Marine and Petroleum Geology*, *73*, 517–527. https://doi.org/10.1016/j.marpetgeo.2016.03.002

Abdullayev, N. R., Riley, G. W., & Bowman, A. (2012) Regional controls on lacustrine sandstone reservoirs: The Pliocene of the South Caspian Basin. In O. W. Baganz, Y. Bartov, K. Bohacs, & D. Nummedal (Ed.), *Lacustrine sandstone reservoirs and hydrocarbon systems*. American Association of Petroleum Geologists, Memoir, *95*, 71–98.

Abreu, V., & Nummedal, D. (2007) Miocene to quaternary sequence stratigraphy of the south and central Caspian basins. In P. O. Yilmaz & G. H. Isaksen (Eds.), *Oil and gas of the greater Caspian area, Tulsa*. AAPG Studies in Geology, *55*, 65–86.

Aliyev, A. G. (1949). Petrography of the Tertiary sediments of Azerbaijan, Aznefteizdat Baku (in Russian).

Aliyeva, E. G., Aliyev, C. A., Huseynov, D. A., Babayev, S., & Mamedov, R. (2008). Depositional environment of the lower portion of the Productive Series sediments and their natural radioactivity. *Stratigraphy and Sedimentology of Oil-Gas Basins*, *2*, 91–110.

Allen, M. B., Morton, A. C., Fanning, C., Ismail-Zadeh, A. J., & Kronenberg, S. B. (2006). Zircon age constraints on sediment provenance in the Caspian region. *Journal of the Geological Society*, *163*(4), 647–655. https://doi.org/10.1144/0016-764920-068

Allen, M. B., Vincent, A. C., Alsop, I. A., Ismail-Zade, A., & Flecker, R. (2003). Late Cenozoic deformation in the South Caspian region: Effects of the rigid basement bloc within the collision zone. *Tectonophysics*, *366*, 223–239. https://doi.org/10.1016/S0040-1951(03)00098-2

Amidon, W. H., Burbank, D. W., & Gehrels, G. E. (2005a). U-Pb zircon ages as a sediment mixing tracer in the Nepal Himalaya. *Earth and Planetary Science Letters*, *235*(1), 244–260. https://doi.org/10.1016/j.epsl.2005.03.019

Amidon, W. H., Burbank, D. W., & Gehrels, G. E. (2005b). Construction of detrital mineral populations: Insights from mixing of U-Pb zircon ages in Himalayan rivers. *Basin Research*, *17*(4), 463–485. https://doi.org/10.1111/j.1365-2117.2005.00279.x

Avdeev, B. (2011). Tectonics of the Greater Caucasus and the Arabia-Eurasia orogen. Ph.D. Thesis. University of Michigan.

Avdeev, B., & Niemi, N. A. (2011). Rapid Pliocene exhumation of the central Greater Caucasus constrained by low-temperature thermochronology. *Tectonics*, *30*(2).

Azizbekov, S. A. (1972). *Geology of the USSR: Azerbaijan SSR*. Moscow, Russia: Nedra.

Baturin, V. P. (1937). Paleogeography on the base of terrigenous components. Baku, Moscow (in Russian with English summary), AzONTI, Baku, 291.

Bidgoli, T. S., Amir, E., Walker, D., Stockli, D. F., Andrew, J. E., & Caskey, J. (2015). Low-temperature thermochronology of the Black and Panamint mountains, Death Valley, California: Implications for geodynamic controls on Cenozoic intraplate strain. *Lithosphere*, *7*(4), 473–480. https://doi.org/10.1130/L406.1

Black, L. P., Kamo, S. L., Allen, C. M., Davis, D. W., Aleinikoff, J. N., Valley, J. W., … Foudoulis, C. (2004). Improved ^{206} Pb/^{238}U microprobe geochronology by the monitoring of a trace-element-related matrix effect; SHRIMP, ID–TIMS, ELA–ICP–MS and oxygen isotope documentation for a series of zircon standards. *Chemical Geology*, *205*, 115–140. https://doi.org/10.1016/j.chemgeo.2004.01.003

Blackburn, T. J., Stockli, D. F., Carlson, R. W., & Berendsen, P. (2008). (U-Th)/He dating of kimberlites–A case study from northeastern Kansas. *Earth and Planetary Science Letters*, *275*, 111–120. https://doi.org/10.1016/j.epsl.2008.08.006

Bradley, D., Haeussler, P., O'Sullivan, P., Friedman, R., Till, A., Bradley, D., & Trop, J. (2009). Detrital zircon geochronology of Cretaceous and Paleogene strata across the south-central Alaskan convergent margin. In P. J. Haeussler & J. P. Galloway (Eds.), *Studies by the U.S. Geological Survey in Alaska, 2007*. U.S. Geological Survey Professional Paper 1760-F, 36.

Buryakovsky, L., Chilingar, G. V., & Aminzadeh, F. (2001). *Petroleum geology of the South Caspian Basin*. Oxford, UK: Gulf Professional Publishing.

Chang, L., Vasiliev, I., van Baak, C. G. C., Krijgsman, W., Dekkers, M. J., & Roberts, A. P. (2014). Identification and environmental interpretation of diagenetic and biogenic greigite in sediments: A lesson from the Messinian Black Sea. *Geochemistry, Geophysics, Geosystems*, *15*, 3612–3627. https://doi.org/10.1002/2014gc005411

Chang, Z., Vervoost, J. D., McClelland, W. C., & Knaack, C. (2006). U/Pb dating of zircon by LA-ICP-MS. *Geochemistry, Geophysics, Geosystems*, *7*, 1–14.

Chew, D. M., & Donelick, R. A. (2012). Combined apatite fission track and U/Pb dating by LA-ICP-MS and its application in apatite provenance analysis. *Quantitative Mineralogy and Microanalysis of Sediments and Sedimentary Rocks: Mineralogical Association of Canada, Short Course*, *42*, 219–247.

Cowgill, E., Forte, A. M., Niemi, N., Avdeev, B., Tye, A., Trexler, C., … Gogoladze, T. (2016). Relict basin closure and crustal shortening budgets during continental collision: An example from Caucasus sediment provenance. *Tectonics*, *35*(12), 2918–2948. https://doi.org/10.1002/2016TC004295

Devlin, W., Cogswell, J., Gaskins, G., Isaksen, G., Pitcher, D., Puls, D., … Wall, G. (1999). South Caspian Basin: Young, cool, and full of promise. *GSA Today*, *9*(7), 1–9.

Dickinson, W. R., & Gehrels, G. E. (2009). U/Pb ages of detrital zircons in Jurassic eolian and associated sandstones of the Colorado Plateau: Evidence for transcontinental dispersal and intraregional recycling of sediment. *GSA Bulletin*, *121*, 408–433. https://doi.org/10.1130/B26406.1

Dilek, Y., Imamverdiyev, N., & Atunkaynak, S. (2010). Geochemistry and tectonics of Cenozoic volcanism in the Lesser Caucasus (Azerbaijan) and the peri-Arabian region: Collision-induced mantle dynamics and its magmatic fingerprint. *International Geology Review*, *52*(4–6), 536–578. https://doi.org/10.1080/00206810903360422

Donelick, R. A., O'Sullivan, P. B., & Ketcham, R. A. (2005). Apatite fission-track analysis. *Reviews in Mineralogy and Geochemistry*, *58*(1), 49–94. https://doi.org/10.2138/rmg.2005.58.3

Dunkle, S. S., Helmich, R. J., & Suslick, K. S. (2009). BiVO4 as a visible-light photocatalyst prepared by ultrasonic spray pyrolysis. *The Journal of Physical Chemistry C*, *113*(28), 11980–11983. https://doi.org/10.1021/jp903757x

Farley, K. A. (2002). (U–Th)/He dating: Techniques, calibrations, and applications. *Reviews in Mineralogy and Geochemistry*, *47*, 819–844. https://doi.org/10.2138/rmg.2002.47.18

Farley, K. A., Wolf, R. A., & Silver, L. T. (1996). The effects of long alpha-stopping distances on (U-Th)/He ages. *Geochimica et Cosmochimica Acta*, *60*(21), 4223–4229. https://doi.org/10.1016/S0016-7037(96)00193-7

Figueiredo, J., Hoorn, C., van Der Ven, P., & Soares, E. (2009). Late Miocene onset of the Amazon River and the Amazon deep-sea fan: Evidence from the Foz do Amazonas Basin. *Geology*, *37*(7), 619–622. https://doi.org/10.1130/G25567A.1

Flowers, R. M., & Farley, K. A. (2012). Apatite 4He/3He and (U-Th)/He evidence for an ancient Grand Canyon. *Science*, *338*(6114), 1616–1619. https://doi.org/10.1126/science.1229390

Forte, A. M., Summer, D. Y., Cowgill, E., Stoica, M., Murtuzayev, I., Kangarli, T., … Javakhishvili, Z. (2015). Late Miocene to Pliocene Stratigraphy of the Kura Basin, a subbasin of the South Caspian Basin: Implications for the diachroneity of the stage boundaries. *Basin Research*, *27*, 247–271. https://doi.org/10.1111/bre.12069

Gehrels, G. E., Dickinson, W. R., Ross, G. M., Stewart, J. H., & Howell, D. G. (1995). Detrital zircon reference for Cambrian to Triassic miogeoclinal strata of western North America. *Geology*, *23*(9), 831–834. https://doi.org/10.1130/0091-7613(1995)023<0831:DZRFCT>2.3.CO;2

Gehrels, G., Kapp, P., Decelles, P., Pullen, A., Blakey, R., Weislogel, A., … Yin, A. (2011). Detrital zircon geochronology of pre-Tertiary strata in the Tibetan-Himalayan orogen. *Tectonics*, *30*(5), 1–27.

Gehrels, G. E., Valencia, V. A., & Ruiz, J. (2008). Enhanced precision, accuracy, efficiency, and spatial resolution of U-Pb ages by laser ablation–multicollector–inductively coupled plasma–mass spectrometry. *Geochemistry, Geophysics, Geosystems*, *9*(3), 1–13.

Green, T., Abdullayev, N., Hossack, J., Riley, G., & Roberts, A. M. (2009). Sedimentation and Subsidence in the South Caspian Basin, Azerbaijan. In M.-F. Brunet, M. Wilmsen, & J. W. Granath (Eds.), *South Caspian to Central Iran Basins*. Geological Society of London Special Publication, London, *312*, 241–260.

Hay, W. W., Sloan, J. L., & Wold, C. N. (1988). Mass/age distribution and composition of sediments on the ocean floor and the global rate of sediment subduction. *Journal of Geophysical Research*, *93*, 14933–14940. https://doi.org/10.1029/JB093iB12p14933

Hilgen, F. J., Lourens, L. J., & van Dam, J. A. (2012). The neogene period. In F. Gradstein, J. Ogg, M. Schmitz, & G. Ogg (Eds.), *The geological time scale*. Amsterdam, the Netherlands: Elsevier.

Hinds, D. J., Simmons, M., Allen, M. B., & Aliyeva, E. (2007) Architecture variability in the Pereriva and Balakhany Suites of the neogene productive series, Azerbaijan: Implications for reservoir quality. In P. O. Yilmaz & G. H. Isaksen (Eds.), *Oil and gas of the Greater Caspian area*. American Association of Petroleum Geologists Studies in Geology, *55*, 87–107.

Hultz, C. P., Wilson, H., Donelick, R. A., & O'Sullivan, P. B. (2013). Two flysch belts having distinctly different provenance suggest no stratigraphic link between the Wrangellia composite terrane and the paleo-Alaskan margin. *Lithosphere*, *5*(6), 575–594. https://doi.org/10.1130/l310.1

Jones, R. W., & Simmons, M. D. (1996). A review of stratigraphy of eastern Paratethys (Oligocene–Holocene). *Bulletin of the Natural History Museum London (Geology)*, *52*, 25–49.

Khain, V. Y. (1975). Principle stages of tectonic magmatic development of the Caucasus and experiment in geodynamical interpretation. *Geotectonics*, *1*, 6–13.

Kral, J., & Gurbanov, A. G. (1996). Apatite fission track data from the great caucasus pre-alpine basement. *Chemie Der Erde*, *56*, 177–192.

Krijgsman, W., Stoica, M., Vasiliev, I., & Popov, V. V. (2010). Rise and fall of the Paratethys Sea during the Messinian Salinity Crisis. *Earth and Planetary Science Letters*, *290*, 183–191. https://doi.org/10.1016/j.epsl.2009.12.020

Lanphere, M. A., & Baadsraard, H. (2001). Precise K-Ar, $^{40}Ar/^{39}Ar$, Rb-Sr and U-Pb mineral ages from the 27.5 Ma Fish Canyon Tuff reference standard. *Chemical Geology*, *175*, 653–671. https://doi.org/10.1016/S0009-2541(00)00291-6

McClusky, S., Balassanian, S., Barka, A., Demir, C., Ergintav, S., Georgiev, I., … Kastens, K. (2000). Global Positioning System constraints on plate kinematics and dynamics in the eastern Mediterranean and Caucasus. *Journal of Geophysical Research: Solid Earth*, *105*(B3), 5695–5719. https://doi.org/10.1029/1999JB900351

Metivier, F., Gaudemer, Y., Tapponnier, P., & Klein, M. (1999). Mass accumulation rates in Asia during the *Cenozoic*. *Geophysical Journal International*, *137*, 280–318.

Molnar, P. (2004). Late Cenozoic increase in accumulation rates of terrestrial sediment: How might climate change have affected erosion rates? *Annual Review of Earth and Planetary Sciences*, *32*, 67–89. https://doi.org/10.1146/annurev.earth.32.091003.143456

Moore, T. E., O'Sullivan, P. B., Potter, C. J., & Donelick, R. A. (2015). Provenance and detrital zircon geochonologic evolution of lower Brookian foreland basin deposits of the western Brooks Range, Alaska, and implications for early Brookian tectonism. *Geosphere*, *11*, 93–122. https://doi.org/10.1130/ges01043.1

Morton, A., Allen, M., Simmons, M., Spathopoulos, F., Still, J., Hinds, D., … Kroonenberg, S. (2003). Provenance patterns in a neotectonic basin: Pliocene and quaternary sediment supply to the South Caspian. *Basin Research*, *15*, 321–337. https://doi.org/10.1046/j.1365-2117.2003.00208.x

Mosar, J., Kangarli, T., Bochud, M., Glasmacher, U., Rast, A., Brunet, M.-F., & Soossn, M. (2010) Cenozoic-recent tectonics and uplift in the greater Caucasus: A perspective from Azerbaijan. In M. Sossonm, N. Kaymakchi, R. A. Stephenson, F. Bergerat, & V. Starostenko (Eds.), *Sedimentary basin tectonics from the black sea and Caucasus to the Arabian platform*. Geological Society, London, Special Publications, *340*, 261–280.

Niemi, N. A., & Avdeev, B. (2010). Differential exhumation across the eastern Greater Caucasus from low-temperature thermochronology: Implications for plate boundary reorganization and foreland basin deformation. American Geophysical Union, Fall Meeting 2010, abstract #T41D-08.

Nummedal, D., Clifton, H. E., & Williams, E. (2012) Late Miocene and early Pliocene high frequency lake level cycles in Lacustrine hydrocarbon reservoir strata: South Caspian Basin: Insights for Subseismic-scale Lithofacies variations. In O. W. Baganz, Y. Bartov, K. Bohacs, & D. Nummedal (Eds.), *Lacustrine sandstone reservoirs and hydrocarbon systems*. American Association of Petroleum Geologists Memoir, *95*, 99–122.

Paces, J. B., & Miller, J. D. (1993). Precise U-Pb ages of Duluth complex and related mafic intrusions, northeastern Minnesota: Geochronological insights to physical, petrogenetic, paleomagnetic, and tectonomagmatic processes associated with the 1.1 Ga midcontinent rift system. *Journal of Geophysical Research: Solid Earth*, *98*(B8), 13997–14013.

Philip, H., CisternaS, A., Givshiani, A., & Gorshkov, A. (1989). The Caucasus: An actual example of the initial stages of continental collision. *Tectonophysics*, *161*, 1–12. https://doi.org/10.1016/0040-1951(89)90297-7

Popov, S. V., Shcherba, I. G., Ilyina, L. B., Nevesskaya, L. A., Paramonova, N. P., Khondkarian, S. O., & Magyar, I. (2006). Late Miocene to Pliocene palaeogeography of the Paratethys and its relation to the Mediterranean. *Palaeogeography, Palaeoclimatology, Palaeoecology*, *238*(1), 91–106. https://doi.org/10.1016/j.palaeo.2006.03.020

Potapov, I. I. (1954). Absheron oil-bearing province (geological characteristic). Academy of Science of Azerbaijan Republic (in Russian).

Puchkov, V. N. (1997). Structure and geodynamics of the Uralian orogen. In J.-P. Burg & M. Ford (Ed.), *Orogeny through time*. Geological Society, London, Special Publications, *121*, 201–236.

Pullen, A., Gehrels, G. E., Ibanez-Mejia, J. C., & Pecha, M. (2014). What happens when n = 1000? Creating large-n geochronological datasets with LA-ICP-MS for geologic investigations *Journal of Analytical Atomic Spectrometry*, *29*, 971–980. https://doi.org/10.1039/c4ja00024b

Reilinger, R., MCClusky, S., Vernan, T. P., Lawrence, S., Ergintav, S., Cakmak, R., … Nadariya, M. (2006). GPS constraints on continental deformation in the Africa-Arabia-Eurasia continental collision zone and implications for the dynamics of plate interactions. *Journal of Geophysical Research: Solid Earth*, *111*(B5), 1–26.

Reiners, P. W., & Shuster, D. L. (2009). Thermochronology and landscape evolution. *Physics Today*, *62*(9), 31–36. https://doi.org/10.1063/1.3226750

Renne, P. R., Swisher, C. C., Deino, A. L., Karner, D. B., Owens, T. L., & Depaolo, D. J. (1998). Intercalibration of standards, absolute ages and uncertainties in $^{40}Ar/^{39}Ar$ dating. *Chemical Geology*, *45*, 117–152. https://doi.org/10.1016/S0009-2541(97)00159-9

Reynolds, A. D., Simmons, M. D., Bowman, M. B. J., Henton, J., Brayshaw, A. C., Ali-Zade, A. A., … Koshkarly, R. O. (1998). Implications of outcrop geology for reservoirs in the Neogene Productive Series: Apsheron Peninsula, Azerbaijan. *American Association of Petroleum Geologists Bulletin*, *82*, 25–49.

Salmanov, A., Suleymanov, A., & Maharramov, B. (2015). *Paleogeology of oil and gas bearing regions in Azerbaijan*. Baku, Azerbaijan: Mars Print.

Satkoski, A. M., Wilkinson, B. H., Hietpas, J., & Samson, S. D. (2013). Likeness among detrital zircon populations — An approach to the comparison of age frequency data in time and space. *GSA Bulletin*, *125*, 1783–1799. https://doi.org/10.1130/b30888.1

Stacey, J. S., & Kramer, J. D. (1975). Approximation of terrestrial lead isotope evolution by a two-stage model. *Earth and Planetary Science Letters*, *26*, 207–221. https://doi.org/10.1016/0012-821X(75)90088-6

Steiger, R. H., & Jäger, E. (1977). Subcommission on geochronology: Convention on the use of decay constants in geo- and cosmochronology. *Earth and Planetary Science Letters*, *36*(3), 359–362. https://doi.org/10.1016/0012-821X(77)90060-7

Stoica, M., Lazar, I., Krijgsman, W., Vasiliev, I., Jipa, D. C., & Floroiu, A. (2013). Palaeoenvironmental evolution of the East Carpathian foredeep during the Late Miocene - Early Pliocene (Dacian Basin; Romania). *Global and Planetary Change*, *103*, 135–148. https://doi.org/10.1016/j.gloplacha.2012.04.004

Sultanov, A. D. (1949). *Lithology of the productive series of Azerbaijan*. Baku, Azerbaijan: Publishing House of the Academy of Sciences of Azerbaijan.

van Baak, C. G. C. (2015). Mediterranean-Paratethys connectivity during the late Miocene to Recent. Ph.D. Thesis. University of Utrecht.

van Baak, C. G. C., Stoica, M., Grothe, A., Aliyeva, E., & Krijgsman, W. (2016). Mediterranean-Paratethys connectivity during the Messinian salinity crisis: The Pontian of Azerbaijan. *Global and Planetary Change*, *141*, 63–81. https://doi.org/10.1016/j.gloplacha.2016.04.005

van Baak, C. G. C., Vasiliev, I., Stoica, M., Kuiper, K. F., Forte, A. M., Aliveva, E., & Krijgsman, W. (2013). A magnetostratigraphic time frame for Plio-Pleistocene transgressions in the South Caspian Basin, Azerbaijan. *Global and Planetary Change*, *103*, 119–134. https://doi.org/10.1016/j.gloplacha.2012.05.004

Vasiliev, I., Krijgsman, W., Langereis, C. G., Panaiotu, C. E., Matenco, L., & Bertotti, G. (2004). Towards an astrochronological framework for the eastern Paratethys Mio-Pliocene sedimentary sequences of the Focsani basin (Romania). *Earth and Planetary Science Letters*, *227*, 231–247. https://doi.org/10.1016/j.epsl.2004.09.012

Vernant, P. H., Nilforoushan, F., Hatzfeld, D., Abbasi, M. R., Vigny, C., Masson, F., … Chery, J. (2004). Present day crustal deformation and plate kinematics in the Middle East constrained by GPS measurements in Iran and northern Oman. *Geophysical Journal International*, *157*, 381–398. https://doi.org/10.1111/j.1365-246X.2004.02222.x

Vincent, S. J., Carter, A., Lavrishchevv, V. A., Rice, S. P., Barabadze, T. G., & Hovius, N. (2011). The exhumation of the western Greater Caucasus: A thermochronometric study. *Geological Magazine*, *148*(1), 1–21. https://doi.org/10.1017/S0016756810000257

Vincent, S. J., Davies, C. E., Richards, K., & Aliyeva, E. (2010). Contrasting pliocene fluvial depositional systems within the rapidly subsiding South Caspian Basin; A case study of the Palaeo-Volga and Palaeo-Kura river systems in the surakhany suite, upper productive series, onshore Azerbaijan. *Marine and Petroleum Geology*, *27*, 2079–2106. https://doi.org/10.1016/j.marpetgeo.2010.09.007

Vincent, S. J., Morton, A. C., Carter, A., Gibbs, S., & Barabadze, T. G. (2007). Oligocene uplift of the Western Greater Caucasus; an effect of initial Arabia-Eurasia collision. *Terra Nova*, *19*, 160–166. https://doi.org/10.1111/j.1365-3121.2007.00731.x

Wang, C. Y., Campbell, I. H., Stepanov, A. S., Allen, C. M., & Burtsev, I. N. (2011). Growth rate of the preserved continental crust: II. Constraints from Hf and O isotopes in detrital zircons from Greater Russian Rivers. *Geochimica et Cosmochimica Acta*, *75*, 1308–1345. https://doi.org/10.1016/j.gca.2010.12.010

Westaway, R. (1994). Present-day kinematics of the Middle East and eastern Mediterranean. *Journal of Geophysical Research*, *99*(B6), 12071–12090. https://doi.org/10.1029/94JB00335

Zhang, P., Molnar, P., & Downs, W. (2001). Increased sedimentation rates and grainsizes 2 ± 4 Myr ago due to the influence of climate change on erosion rates. *Nature*, *410*, 891–897.

Zonenshain, L. P., & Le Pichon, X. (1986). Deep basins of the Black Sea and Caspian Sea as remnants of Mesozoic back-arc basins. *Tectonophysics*, *123*(1), 181–211.

SUPPORTING INFORMATION

Additional Supporting Information may be found online in the supporting information tab for this article.

How to cite this article: Abdullayev NR, Weber J, Aliyeva E, et al. Detrital zircon and apatite constraints on depositional ages, sedimentation rates and provenance: Pliocene Productive Series, South Caspian Basin, Azerbaijan. *Basin Res*. 2018;30:835–862. https://doi.org/10.1111/bre.12283